iScience

CellPress
OPEN ACCESS

Article

A Sustainable Chemicals Manufacturing Paradigm Using CO_2 and Renewable H_2

Rajesh Reddy Bommareddy, Yanming Wang, Nicole Pearcy, Martin Hayes, Edward Lester, Nigel P. Minton, Alex V. Conradie

rajesh.bommareddy@nottingham.ac.uk (R.R.B.)
alex.conradie@nottingham.ac.uk (A.V.C.)

HIGHLIGHTS

Stable and continuous gas fermentation using *C. necator*

Carbon-efficient bio-catalysis from CO_2 and H_2 to commodity chemicals

Heat integration overcomes energy inefficiency of biological CO_2 fixation

Bommareddy et al., iScience *23*, 101218
June 26, 2020
https://doi.org/10.1016/j.isci.2020.101218

iScience

CellPress
OPEN ACCESS

Article

A Sustainable Chemicals Manufacturing Paradigm Using CO_2 and Renewable H_2

Rajesh Reddy Bommareddy,[3,4,6,*] Yanming Wang,[3,4] Nicole Pearcy,[3,5] Martin Hayes,[2] Edward Lester,[1] Nigel P. Minton,[3] and Alex V. Conradie[1,*]

SUMMARY

The chemical industry must decarbonize to align with UN Sustainable Development Goals. A shift toward circular economies makes CO_2 an attractive feedstock for producing chemicals, provided renewable H_2 is available through technologies such as supercritical water (scH_2O) gasification. Furthermore, high carbon and energy efficiency is paramount to favorable techno-economics, which poses a challenge to chemo-catalysis. This study demonstrates continuous gas fermentation of CO_2 and H_2 by the cell factory, *Cupriavidus necator*, to (R,R)-2,3-butanediol and isopropanol as case studies. Although a high carbon efficiency of 0.75 [(C-mol product)/(C-mol CO_2)] is exemplified, the poor energy efficiency of biological CO_2 fixation requires ~8 [(mol H_2)/(mol CO_2)], which is techno-economically infeasible for producing commodity chemicals. Heat integration between exothermic gas fermentation and endothermic scH_2O gasification overcomes this energy inefficiency. This study unlocks the promise of sustainable manufacturing using renewable feedstocks by combining the carbon efficiency of bio-catalysis with energy efficiency enforced through process engineering.

INTRODUCTION

The chemical industry has been central to the modern world since the Industrial Revolution, converting raw materials such as fossil reserves into thousands of products through numerous continuous processes. Although the chemical industry has served economic growth well over many decades, much of the chemical industry has become misaligned with the United Nation's (UN) Sustainable Development Goals, notably Sustainable Industrialization and Climate Action (Axon and James, 2018). Current large-scale manufacturing processes suffer from a reliance on finite fossil reserves, high energy consumption, and poor overall catalytic selectivity. Circular economies are markedly absent and net greenhouse gas emissions exacerbate climate change (Keijer et al., 2019).

Given the chemical industry needs to decarbonize, the use of CO_2 as a carbon feedstock for producing chemicals has significant synergy with UN Sustainable Development Goals, provided a renewable supply of reducing power is available from either H_2 or H_2O. Renewable H_2 can be produced via a number of sustainable technologies, including (1) biomass pyrolysis-gasification (Dou et al., 2019), (2) dark fermentation of complex carbohydrates (Boboescu et al., 2016), (3) supercritical water gasification (Okolie et al., 2019), and (4) megawatt-scale water electrolysis (Schmidt et al., 2017). Such renewable H_2 can be used to produce methanol from CO_2 chemo-catalytically, where a typical reactor has a methanol outlet composition of ~61% by mole of the total carbon products (Toyir et al., 2009). This renewable methanol can be converted to C2–C4 olefin chemical building blocks using SAPO-34 zeolite catalysts, noting a typical reactor has a propene outlet composition of 39% by weight of the total carbon products in commercial practice. In addition to low selectivity, the Methanol to Olefins (MTO) process suffers from rapid catalyst coking, necessitating continuous regeneration of the catalyst within the fluidized bed reactor (Tian et al., 2015). The MTO process' greater selectivity for propene creates opportunities to produce C3 and C4 alcohol solvents. Isopropanol can be produced via the hydration of the C3 propene fraction, whereas C4 alcohols can be produced through hydroformylation of propene using the Oxo^{SM} Process with ~85% selectivity for the linear C4 product over the branched C4 by-product (Tudor and Shah, 2017). In addition to the techno-economic challenges posed by low overall selectivity and catalyst deactivation, the high temperature and pressure processing associated with the chemo-catalytic conversion of CO_2 and H_2 to C3 and C4 products is energy intensive (Toyir et al., 2009; Tian et al., 2015; Tudor and Shah, 2017).

[1]Department of Chemical & Environmental Engineering, University of Nottingham, Nottingham NG7 2RD, UK

[2]Johnson Matthey Technology Centre, 28 Cambridge Science Park, Milton Road, Cambridge CB4 0 FP, UK

[3]BBSRC/EPSRC Synthetic Biology Research Centre, Biodiscovery Institute (BDI), School of Life Sciences, University of Nottingham, Nottingham NG7 2RD, UK

[4]Present address: Department of Chemical & Environmental Engineering, University of Nottingham, Nottingham NG7 2RD, UK

[5]Present address: School of Veterinary Medicine and Science, University of Nottingham, Nottingham LE12 5RD, UK

[6]Lead Contact

*Correspondence: rajesh.bommareddy@nottingham.ac.uk (R.R.B.), alex.conradie@nottingham.ac.uk (A.V.C.)

https://doi.org/10.1016/j.isci.2020.101218

Microbial cell factories produce biocatalysts (enzymes) and use the cell's energy carriers to synthesize products via these non-native biochemical pathways. Such bio-catalysis presents opportunities to reinvent chemicals manufacturing using sustainable feedstocks and renewable energy, harnessing the high catalytic selectively of microbial cell factories at low temperature and pressure (Hedstrom, 2010). Although several acetogenic cell factories are able to fix CO_2 using H_2 anaerobically, these cell factory platforms suffer from energetic limitations (Molitor et al., 2017) and the production of fermentative by-products such as acetate (Hoffmeister et al., 2016). Conversely, *Cupriavidus necator* (formerly, *Alcaligenes eutrophus* and *Ralstonia eutropha*) is a chemolithoautotrophic bacterium capable of aerobic, autotrophic growth using CO_2 as the sole carbon source, H_2 as electron donor, and O_2 as the electron acceptor (Brigham, 2019). When the genes producing *C. necator*'s natural carbon sink, polyhydroxybutyrate (phb), are attenuated, the cell accumulates pyruvate as the central metabolite under nutrient limitation, which can be redirected to a number of different carbon products (Steinbüchel and Schlegel, 1989). Consequently, metabolic engineering of *C. necator* to produce chemicals from CO_2 and H_2 has demonstrated promise, most notably in the production of (1) 2-hydroxyisobutyrate for Plexiglas (Przybylski et al., 2012), (2) isobutanol (Brigham et al., 2013), (3) 3-methyl-1-butanol (Li et al., 2012), (4) methyl ketones (Müller et al., 2013), (5) isopropanol (Marc et al., 2017), (6) α-humulene (Krieg et al., 2018), and (7) acetoin (Windhorst and Gescher, 2019). These studies have contributed appreciably to advancing the metabolic engineering of *C. necator* as a platform for using CO_2 as a carbon feedstock, noting that the focus was not on process engineering considerations. As such, these studies were demonstrated at low cell density in batch operation, which is not aligned techno-economically with continuous manufacturing. Additionally, these studies have not addressed the energy inefficiency of biological CO_2 fixation, where the high H_2 utilization makes the process techno-economically infeasible for producing commodity chemicals (Emerson and Stephanopoulos, 2019).

The objective of this study has been to demonstrate integrated, continuous production of chemicals from CO_2 using *C. necator* as the microbial cell factory. Aligning with the continuous operating paradigm of the chemical industry, this paper is the first to demonstrate the stable and continuous bio-manufacture of chemicals from CO_2 using *C. necator* as carbon-efficient cell factory. Furthermore, this study is the first to demonstrate the use of process engineering to overcome the techno-economic hurdle associated with the energy inefficiency of biological CO_2 fixation. The following sections outline the metabolic engineering, continuous gas fermentation, and rigorous process simulation, which exemplify carbon and energy-efficient continuous bio-manufacture through two case studies producing (R,R)-2,3-butanediol (BDO) and isopropanol (IPA).

RESULTS

Metabolic Engineering

Microbial cell factories are able to produce a large number of products via their biochemical networks from a variety of carbon feedstocks. BDO and IPA were selected as the two case studies for continuous autotrophic fermentation in this work, given both biochemical pathways have been extensively characterized (Ji et al., 2011; Marc et al., 2017). The biochemical pathways that convert the central metabolite pyruvate to either BDO or IPA are detailed in Figure 1A. The biochemical pathway genes depicted in Figure 1B were overexpressed as a single operon from either a plasmid or chromosomal integration, employing the synthetic biology methods described in the Transparent Methods section.

C. necator's natural carbon sink pathway to polyhydroxybutyrate (phb) was knocked out by deleting the operon *phaC1AB1* for the BDO cell factory and the genes *phaC1B1* for the IPA cell factory (Peplinski et al., 2010; Raberg et al., 2014; Müller et al., 2013), thereby redirecting carbon flux and reducing equivalents to the fermentation product. Also, given the reported degradation of BDO's precursor acetoin by *C. necator* via what would constitute a competing pathway (Fründ et al., 1989), the *acoXABC* gene cluster was deleted in the BDO cell factory.

The performance evaluations of these BDO and IPA cell factories in heterotrophic shake flask culture are summarized in Table 1 and Figure 2, demonstrating the carbon split using fructose as carbon source. Given that chromosomal integration is associated with greater genetic stability in *C. necator* (Voss and Steinbüchel, 2006; Gruber et al., 2014), the performance of the expressed operons (Figure 1B) was assessed for both plasmid-based and chromosomally integrated cell factories. The cumulative specific fructose uptake rate was comparable across plasmid, integrated and control strains, where the biomass synthesis was controlled via nitrogen limitation. In shake flasks, the integrated BDO cell factory had similar yield and

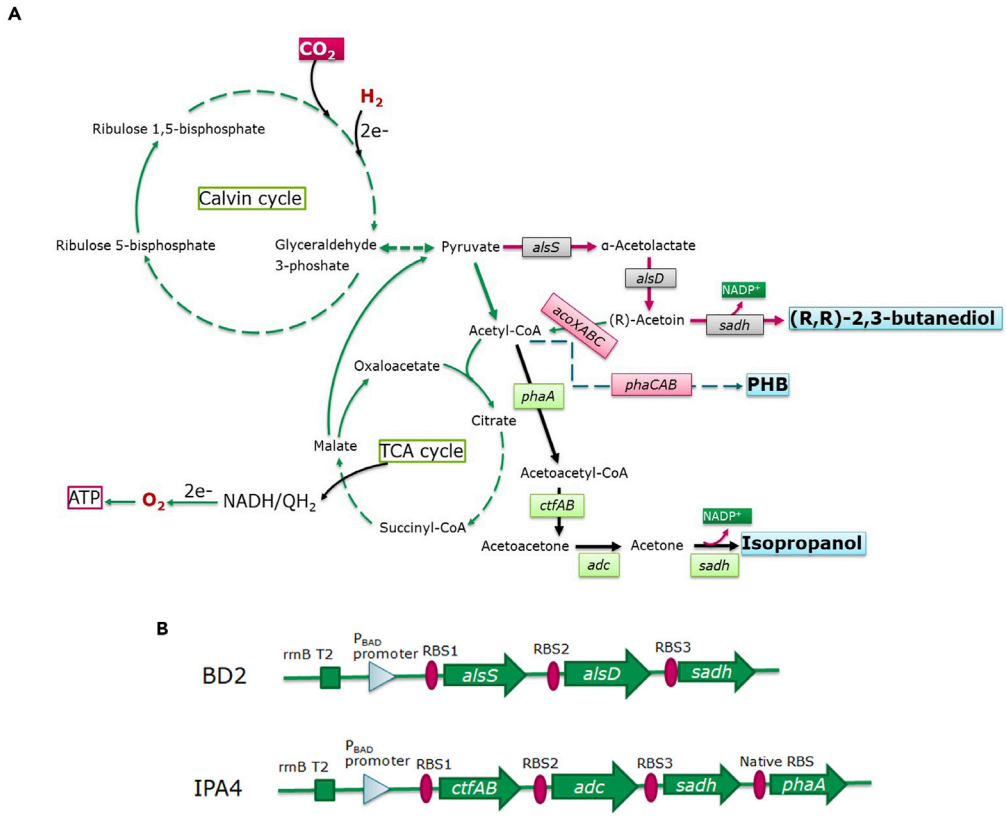

Figure 1. Biochemical Network and Pathway Operons for the Synthesis of (R,R)-2,3-butanediol and isopropanol
(A) Biochemical network outlining the synthesis of (R,R)-2,3-butanediol and isopropanol in the microbial cell factory, *C. necator* H16, converting CO_2 and H_2 to pyruvate via the Calvin Cycle and redirecting carbon flux from pyruvate to (R,R)-2,3-butanediol and isopropanol as case studies. Attenuated genes are contained in red text boxes. Genes overexpressed to allow (R,R)-2,3-butanediol synthesis are contained in gray text boxes, whereas genes overexpressed for isopropanol synthesis are contained in green text boxes.
(B) Pathway operons for BDO (BD2) and isopropanol (IPA4)-producing strains. Both operons rely on pBAD as inducible promoter with ribosome-binding sites as per Table S2 and genes as per Table S4, noting that *phaA* is the native open reading frame.

productivity performance to the plasmid-based cell factory, whereas the IPA plasmid-based cell factory outperformed the integrated cell factory. The greater genetic stability of integrated cell factories is best suited to continuous fermentation, and a single copy integration also provided for a better comparison of performance between BDO and IPA. Therefore, both the BDO and IPA integrated cell factories were taken forward into continuous fermentation using CO_2 and H_2 as per the Transparent Methods section.

Continuous Gas Fermentation

Microorganisms often show reduced tolerance to the accumulation of solvent products such as BDO or IPA. Increasing IPA concentrations in fermentation are detrimental to *C. necator*'s growth above 15 g/L (Marc et al., 2017), recognizing that stripping of IPA into the bioreactor's off-gas increases as the aqueous concentration increases. Also, in continuous fermentation, the IPA is further diluted from the bioreactor. The low volatility of BDO makes its accumulation in the bioreactor's aqueous phase a greater concern. Consequently, shake flask experiments revealed that, above a BDO concentration of 30 g/L, the growth rate of *C. necator* H16 is impaired (Figure S1). Therefore, without resorting to genetic modification, the BDO concentration in continuous bioreactors needs to be controlled through dilution alone.

The continuous, autotrophic fermentation results were generated using the bioreactor experimental setup shown in Figure 3, outlining the decoupled, multi-loop SISO (single-input, single-output) process control strategy for intensifying the process within the flammability safety constraints. The specific CO_2 uptake

Performance Parameter	Unit	2,3-Butanediol			Isopropanol		
		Plasmid	Integrated	Host	Plasmid	Integrated	Host
Cumulative specific fructose uptake rate	[(mmol C)/((g DCW)·h)]	9.6 ± 1.3	9.7 ± 1.2	8.8 ± 1.1	10.2 ± 1.8	9.9 ± 1.6	9.1 ± 1.1
Cumulative molar carbon efficiency (yield)	[(C-mol product)/(C-mol fructose)]	Figure 2					
Final product titer in liquid phase	[g/L]	1.9 ± 0.1	1.8 ± 0.1	nd	2.7 ± 0.2	1.8 ± 0.2	nd

Table 1. Microbial Cell Factory Performance in Heterotrophic Shake Flasks for (R,R)-2,3-Butanediol and Isopropanol Synthesis (Triplicate Biological Replicates)
nd designates not detected.

rates and specific productivities on a biomass (DCW) basis are trended in Figure 4, thereby allowing for comparison between BDO and IPA synthesis against the *ΔphaC1AB1 ΔacoXABC* control strain. For the BDO cell factory, meso-2,3-butanediol is the principal by-product, indicative of promiscuous *secondary alcohol dehydrogenase* activity accepting acetoin as substrate. Acetone is the principal by-product for the IPA cell factory, indicating that the *secondary alcohol dehydrogenase* is the rate-limiting step in the assembled pathway. The control strain produces no products or by-products. The molar ratios of H_2 and O_2 uptake to CO_2 uptake reflect the specific requirement for H_2 as electron donor and O_2 as electron acceptor (Figure 5). The steady-state CO_2 uptake rate for both case studies demonstrated a specific uptake rate of 3–4 ([(mmol C)/(gDCW·h)], consuming ~8 [(mol H_2)/(mol CO_2)] and 2–3 [(mol O_2)/(mol CO_2)]. An ~8 [(mol H_2)/(mol CO_2)]) molar ratio reflects the reducing power required to fix CO_2 and produce the product, generating significant heat owed to the exothermic reaction. Alongside this measure of energy efficiency, the carbon split to product, by-product, and biomass summarizes the carbon efficiency (Table 2 and Figure 6). As such, these data are the first to demonstrate genetically stable and continuous production in *C. necator* via chromosomal integration of non-native genes. The calculation methodology for gas uptake rates, steady-state dilution rate, and carbon fluxes for the continuous, autotrophic fermentations is described in Figure S2. Given the results in Figures 4 and 5 represent calculated data incorporating several sensors, analyses, and calibration standards, two thousand Monte Carlo simulations were undertaken to determine the 90% confidence limits denoted by error bars in Figures 4 and 5. The histogram outputs from the Monte Carlo simulations are contained in Figure S3.

Process Simulation and Systems Biology

Heat Integration of Gas Fermentation with Supercritical Water Gasification

Gas fermentation is a highly exothermic process owed to the cascade of electrons through the biochemical network (Figure 1A) from the electron donor, H_2, to the final electron acceptor, O_2 (Tanaka et al., 1995). The CO_2 is reduced to a number of carbon sinks, typically biomass, the fermentation product, and by-products. Supercritical water (scH_2O) gasification is a hydrothermal technology converting renewable carbon feedstocks, such as wet lignin biomass, to CO_2 and H_2 at supercritical pressure and temperature, i.e., 240 bar (a) and 375°C (Rodriguez Correa and Kruse, 2018). The process is highly endothermic and the renewable H_2 produced by the scH_2O reactor originates from both the hydrocarbon feedstock and the scH_2O. A heat pump can be employed to facilitate the energy (heat) flow from a low temperature (gas fermentation) to a high temperature (scH_2O gasification) via a thermal cycle. The integrated process was rigorously simulated in Aspen HYSYS, summarized in Figure 7 and detailed in Figure 8 using the lignin model compound, guaiacol, as the waste carbon feedstock. From the heat pump cycle depicted in Figure 7, a suitable heat carrying fluid (isopentane) is evaporated at low pressure in an evaporator by the bioreactor's heat of reaction (4,004 kW/ton guaiacol), resulting in a substantial increase in the isopentane's enthalpy (energy) at constant temperature. The isopentane vapor is compressed to a higher pressure via a compressor, further increasing the isopentane's enthalpy owed to the heat of compression (175 kW/ton guaiacol). Further energy is transferred to the vapor via a series of heat exchangers. The scH_2O Recovery Heat Exchanger recovers heat from the scH_2O reactor's effluent (5,565 kW/ton guaiacol), and the Heat Pump Recovery Heat Exchanger recovers heat from the isopentane returning after heating the scH2O reactor feed to supercritical temperature. Thereafter, the temperature of the isopentane is greatly increased in a combustion chamber (3,952 kW/ton guaiacol), fired by a fraction of the renewable H_2 generated

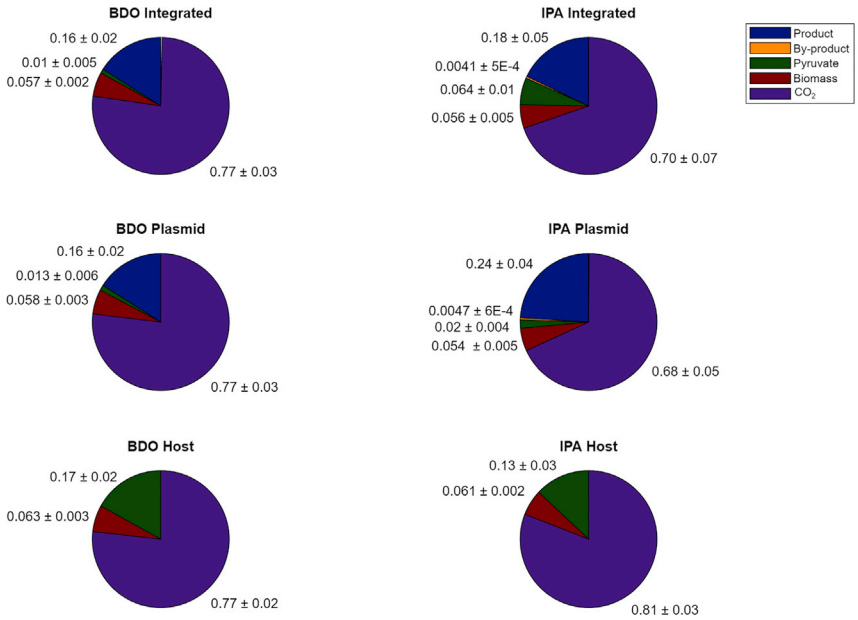

Figure 2. Carbon Efficiency for BDO and IPA Strains in Shake Flask Culture

Cumulative molar carbon efficiency (yield) of microbial cell factories in heterotrophic shake flasks (triplicate biological replicates), representing the carbon split using fructose as carbon source in [(C-mol product)/(C-mol fructose)]. The by-product for the BDO strains is meso-2,3-butanediol and for the IPA strains is acetone. The CO_2 carbon split has been estimated from the carbon balance, noting that the analysis excludes losses of volatile products and by-products to the gas phase. The desired product comprises less than 25% of the carbon from fructose, given the required reducing power that needs to be derived from fructose. Table 1 summarizes additional performance parameters.

in the scH_2O reactor. The high temperature of the isopentane allows heat transfer to the subcritical aqueous feed (3,660 kW/ton guaiacol), raising the sub-critical feed to the scH_2O reactor to supercritical conditions. After the Heat Pump Recovery Heat Exchanger, the vapor is condensed in a condenser (scH_2O Reactor Pre-heater), which pre-heats the feed to the scH_2O reactor (10,036 kW/ton guaiacol). Finally, the liquid isopentane is expanded to lower pressure over a valve for evaporation in the Heat Pump Evaporator by the bioreactor's heat of reaction. The thermal cycle linking the low-temperature energy source, i.e., the exothermic gas fermentation, and the high-temperature energy sink, i.e., the endothermic scH_2O gasification, is subsequently repeated.

The process integration into the heat pump cycle of (1) the combustion chamber, (2) air compression via a turbo-expander, and (3) renewable energy generation via a turbine is detailed in Figure 8. The integrated process was rigorously simulated in Aspen HYSYS, feeding the waste carbon from the High-Pressure Pump (339 kW/ton guaiacol) to the scH_2O Reactor, where CO_2 and H_2 are generated from the carbon feedstock modeled as the lignin model compound, guaiacol. The high-pressure CO_2 & H_2 stream is expanded over the turbo-expander, using the generated 575 kW/ton guaiacol to compress air as the oxygen source for gas fermentation and the combustion chamber. A fraction of the depressurized CO_2 and H_2 and a fraction of the compressed air are fed to the loop bioreactor, where the bleed and permeate fermentation products are produced. The unreacted CO_2 & H_2 in the off-gas from the loop bioreactor is combined with the remaining fraction of the depressurized CO_2 and H_2 to fire the combustion chamber. The combustion chamber's off-gas is fed to a turbine producing renewable electricity (566 kW/ton guaiacol). The scH_2O reactor's effluent is depressurized to release the CO_2 that remained soluble at high pressure, after which the hot aqueous solution can be used for biomass hot water extraction.

Systems Biology for BDO Synthesis Using CO_2 & H_2 and Guaiacol as Sole Energy and Carbon Sources

Rather than gasifying lignin, a next best alternative technology within the context of more conventional heterotrophic fermentation would be a process that converts lignin to guaiacol, thereafter converting the guaiacol to BDO via the 3-oxoadipate pathway. Shen et al. (2020) demonstrated that lignin can be selectively converted to guaiacol as an alternate technology to gasification. *C. necator* is capable of degrading

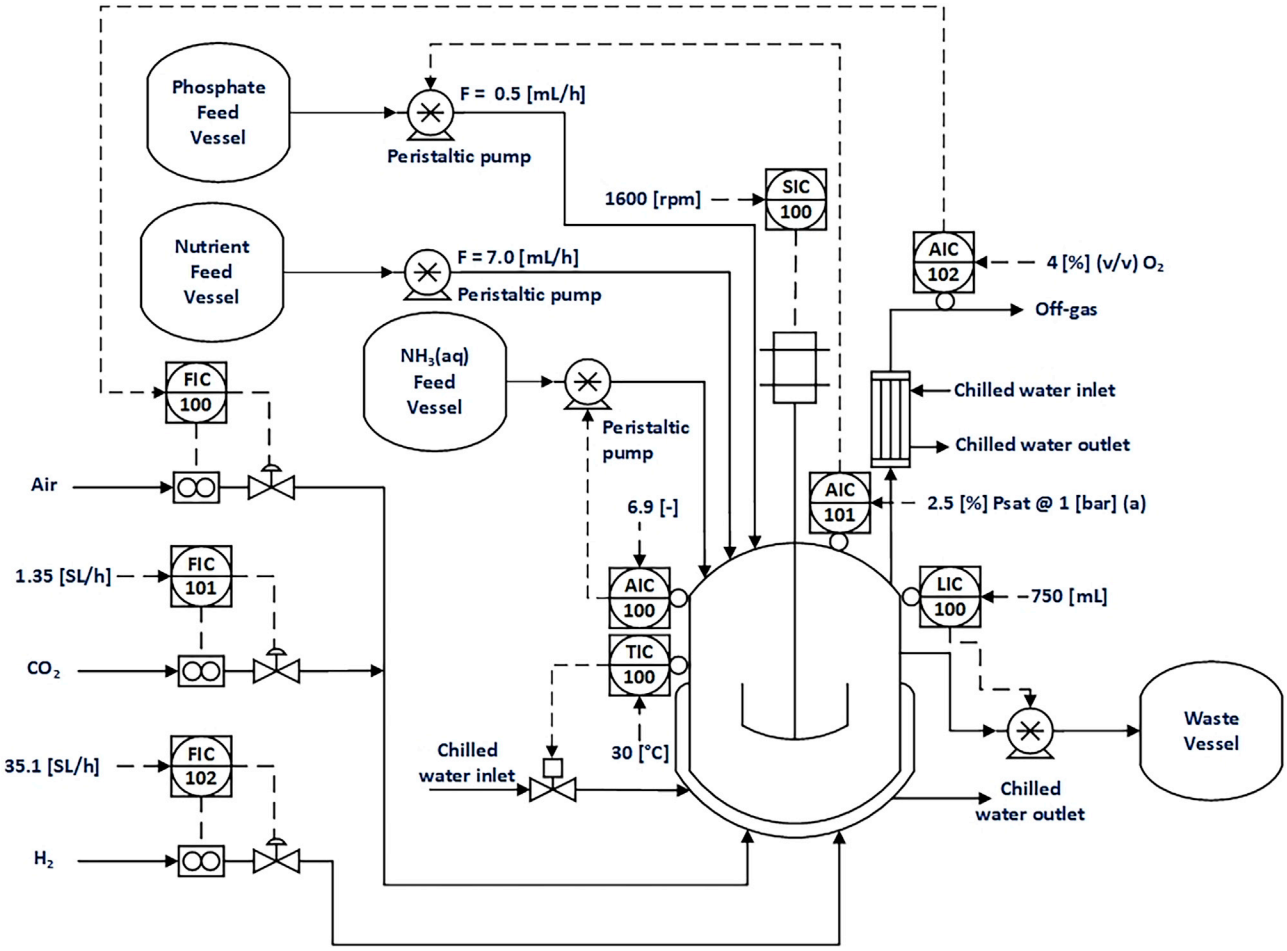

Figure 3. Continuous, Autotrophic Bioreactor Experimental Setup

Continuous bioreactor experimental setup, outlining the decoupled, multi-loop SISO (single-input, single-output) process control strategy for intensifying the continuous autotrophic bioreactor within the flammability safety constraints. The steady-state dissolved oxygen (AIC101) is controlled via the phosphate addition rate, maximizing the process intensification under phosphate limitation. Avoiding a flammable atmosphere in the headspace of the reactor, AIC102 controls the O_2 concentration in the headspace using the air flow.

lignin monomers such as catechol (Wang et al., 2014). However, a microbial cell factory using the lignin model compound guaiacol as the sole energy and carbon source has not been reported. Mallinson et al. (2018) uncovered the *O-demethylase* reaction that allows for guaiacol catabolism in bacteria, characterizing kinetics that suggests guaiacol catabolism is constrained by the conversion of guaiacol to catechol. The required biochemical network for the synthesis of BDO from guaiacol in *C. necator* H16 is shown in Figure S4. Guaiacol is catabolized via the 3-oxoadipate pathway to succinyl-CoA and acetyl-CoA, after which the carbon flux is directed to the cell's TCA cycle. Pyruvate is produced from malate via the *malic enzyme* as the metabolite precursor to BDO synthesis. Using a genome scale model for *C. necator* (Unpublished Data), which advances on the existing model proposed by Park et al. (2011), comparative Flux Balance Analysis (FBA) simulations were run using (1) guaiacol as the sole carbon and energy source and (2) CO_2 and H_2. For CO_2 and H_2, the FBA simulation accurately predicted the O_2 uptake rate, H_2 uptake rate, and the BDO productivity as detailed in Table 2, providing confidence in the predictive power of the genome scale model. The FBA simulation for guaiacol predicted a molar carbon yield of 0.12 [(C mol product)/(C mol guaiacol)] (Table S6). Accordingly, the upstream processing for the guaiacol case was scaled to a guaiacol feed basis of 1,000 kg/h and simulated in Aspen HYSYS as shown for the conventional heterotrophic process flow sheet in Figure 9. Similarly, the upstream processing for the CO_2 & H_2 case was scaled to a guaiacol feed basis of 1,000 kg/h and simulated in Aspen HYSYS as shown for the autotrophic process flow sheet in Figure 8. The bioreactor scale-up for the guaiacol and CO_2 & H_2 Aspen HYSYS simulations is summarized in Table S7.

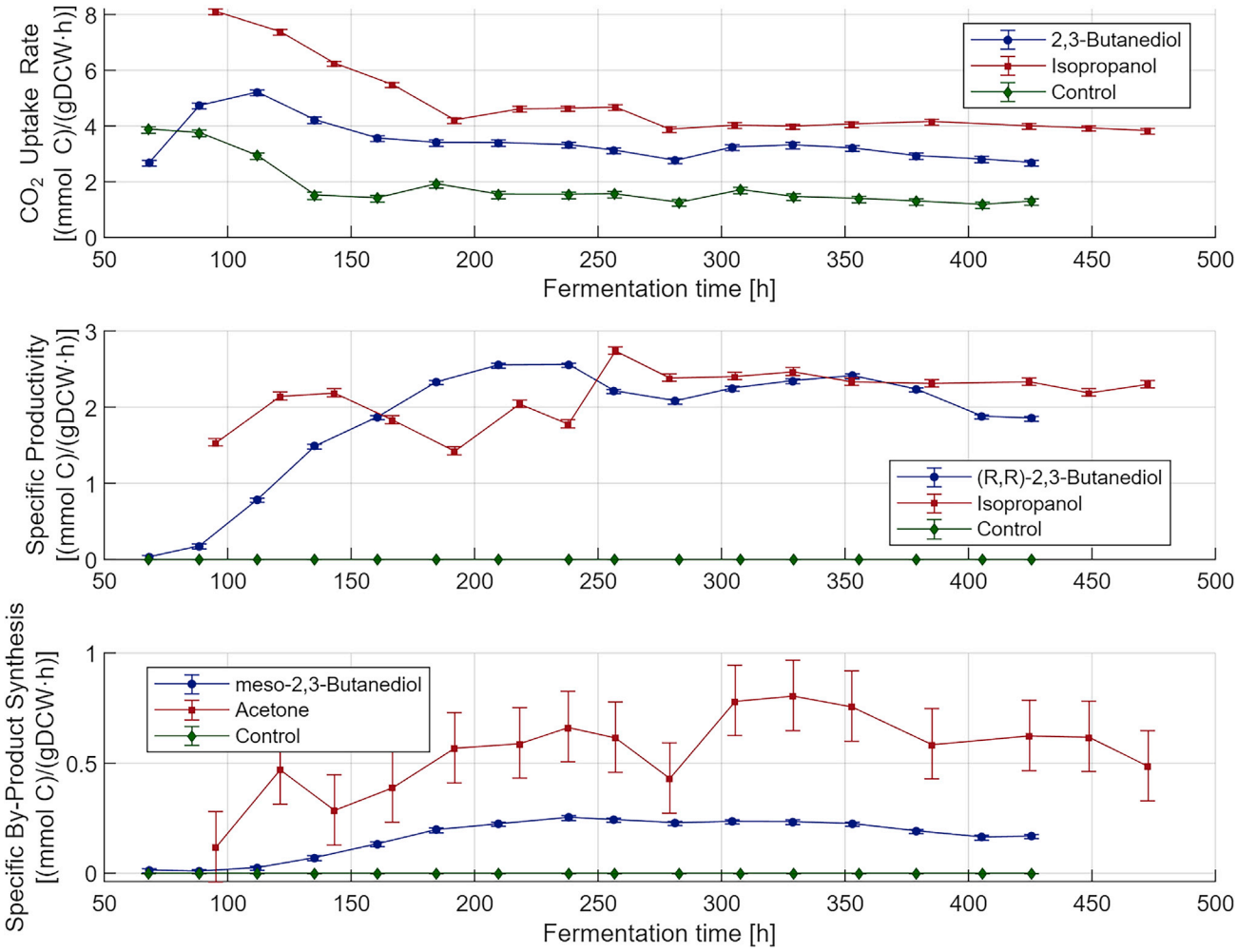

Figure 4. Specific CO_2 uptake rates and specific carbon productivities for continuous, autotrophic fermentations

Specific CO_2 uptake rate (CUR) and specific carbon productivity on a biomass basis during the synthesis of (R,R)-2,3-butanediol and isopropanol in continuous autotrophic fermentation, compared with the *ΔphaC1AB1 ΔacoXABC* control. Specific productivities are comparable, noting the greater carbon overflow to by-product for the isopropanol cell factory. Error bars determined as per Figure S3.

DISCUSSION

High carbon and energy efficiency is essential to achieving favorable techno-economics when converting CO_2 to chemicals, which poses a significant challenge to conventional chemo-catalysis. Principally, the low overall selectivity of the Methanol to Olefin (MTO) process would hamper the sustainable production of C3 and C4 alcohols from CO_2. For the integrated cell factories producing BDO and IPA (Table 1 and Figure 2), the batch experiments using fructose as carbon source showed low molar carbon yields of 0.16–0.18 [(C mol product)/(C mol fructose)]. From Figure 2, the carbon sunk into biomass and by-products was low and a large fraction of carbon was released as CO_2, indicative of the reducing power required for the synthesis of BDO and IPA. Although fructose makes no net contribution to CO_2 emissions, a biogenic carbon source such as lignin would be more cost-effective. However, for the lignin model compound, guaiacol, systems biology simulation for heterotrophic catabolism predicts a similar molar carbon yield of 0.12 [(C mol product)/(C mol guaiacol)]. Scaling this conventional heterotrophic process as in Figure 9 produces 158 kg of BDO per ton of guaiacol, requiring 744 kW of electricity for air compression and 1,638 kW of electricity for the ammonia chiller per ton of guaiacol. The total cooling tower duty amounts to 7,702 kW, adding to the operating cost burden. Despite using renewable feedstocks, such a process could not be described as sustainable.

In contrast, the BDO and IPA cell factories in continuous gas fermentation have substantially improved carbon efficiency, given the reducing power from H_2 is fed separately from the oxidized CO_2 feed. The BDO

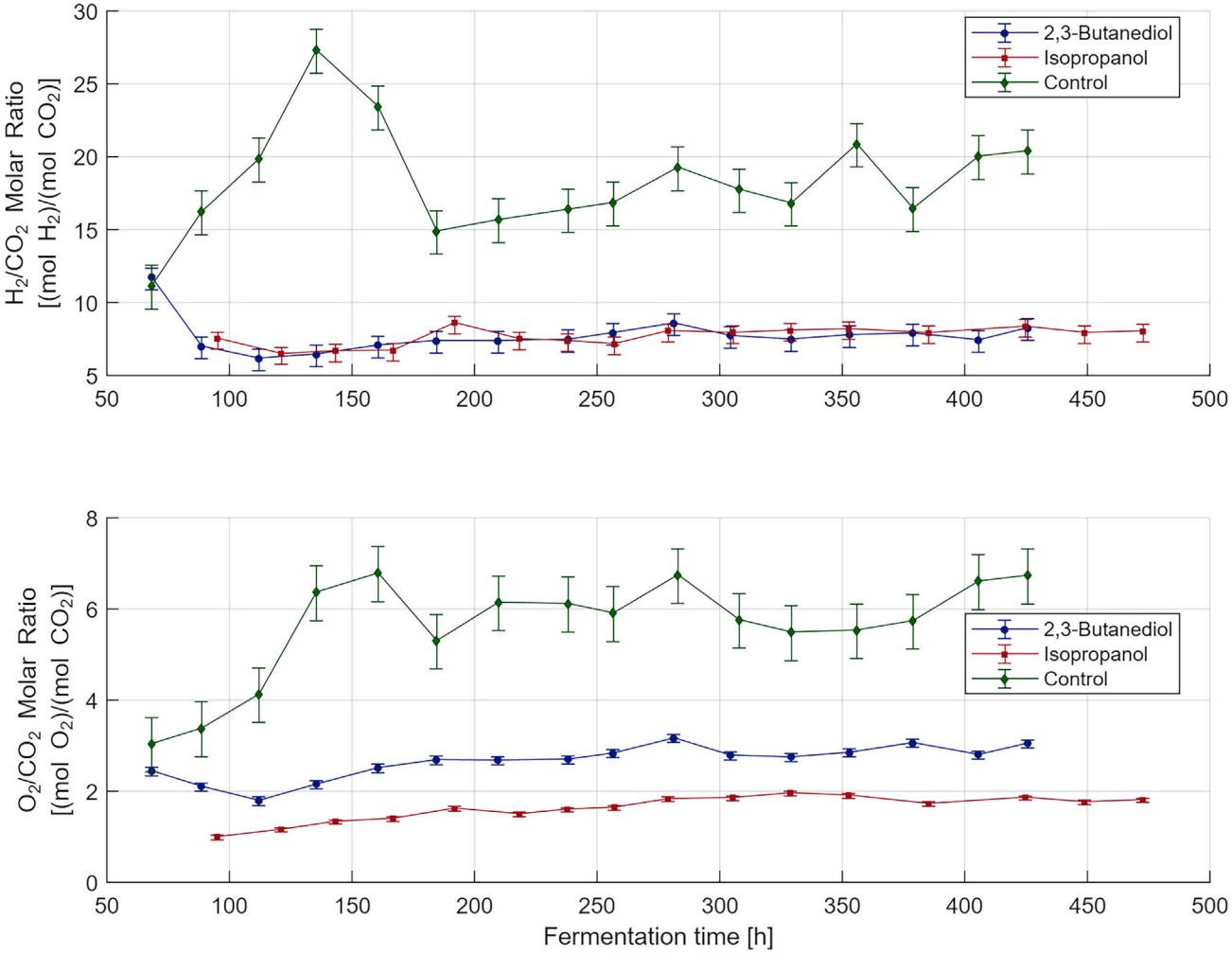

Figure 5. Molar Uptake Ratios for Continuous, Autotrophic Fermentations

Molar uptake ratios for H_2 (electron donor) and O_2 (electron acceptor) to CO_2 during the synthesis of (R,R)-2,3-butanediol and isopropanol in continuous autotrophic fermentation, compared with the *ΔphaC1AB1 ΔacoXABC* control. An ~8 [(mol H_2)/(mol CO_2)] molar ratio reflects the reducing power required to fix CO_2 and produce the product, generating significant heat owed to the exothermic reaction. Error bars determined as per Figure S3.

and IPA cell factories achieved high molar carbon yields of 0.75 [(C mol product)/(C mol CO_2)] and 0.61 [(C mol product)/(C mol CO_2)], respectively (Table 2 and Figure 6), recognizing that the IPA cell factory would benefit from further metabolic engineering optimization. Approximately 0.15–0.2 [(C mol DCW)/(C mol CO_2)] is invested into the continuous production of bio-catalyst, negating the need to have a separate unit operation to regenerate catalyst as for the MTO process. Despite the stable and high overall carbon selectivity (Figures 4 and 6) aligned with the chemical industry's production paradigm, the poor energy efficiency of biological CO_2 fixation requires considerable renewable H_2 at ~8 [(mol H_2)/(mol CO_2)] (Table 2 and Figure 5), which is techno-economically infeasible for producing commodity chemicals.

Several researchers have recognized that the energy inefficiency associated with biological carbon fixation is a hurdle to creating techno-economic processes based on gas fermentation (Bar-Even et al., 2012; Emerson and Stephanopoulos, 2019). The Calvin-Benson-Bassham (CBB) cycle is the dominant carbon fixation pathway given its prevalence within photosynthetic organisms. The CBB cycle's dominance is owed to its advantaged kinetics over other carbon fixation pathways such as the reductive acetyl-CoA pathway prevalent in anaerobic acetogens. This kinetic advantage to reduce CO_2 into biomass and other metabolites comes at a substantial energy cost. For example, to produce 1 mole of acetate, 7.5 moles of H_2 is required by the CBB cycle as opposed to 4 moles of H_2 for the reductive acetyl-CoA pathway (Emerson and Stephanopoulos, 2019). Consequently, a number of augmented and artificial CO_2 fixation pathways have been proposed as a means of improving the energy

Performance Parameter	Unit	BDO[a] Microbial Cell Factory	IPA[b] Microbial Cell Factory
Specific CO_2 uptake rate	[(mmol C)/(gDCW·h)]	3.04 ± 0.12	3.99 ± 0.11
Molar carbon efficiency (yield)	[(C-mol product)/(C-mol CO_2)]	Figure 6	
Carbon balance closure	[%]	102.6	93.7
H_2/CO_2 Molar ratio	[(mol H_2)/(mol CO_2)]	7.91 ± 0.86	8.09 ± 0.74
O_2/CO_2 Molar ratio	[(mol H_2)/(mol CO_2)]	2.92 ± 0.1	1.85 ± 0.06
Product in vapor phase	[-] mole fraction	0	0.75
Product in liquid phase	[g/L]	32.0 ± 0.1	7.7 ± 0.2

Table 2. Microbial Cell Factory Performance in Continuous Autotrophic Fermentation for (R,R)-2,3-Butanediol and Isopropanol Synthesis
[a]BDO is 2,3-butanediol.
[b]IPA is isopropanol.

efficiency of biological C1 fixation cycles. Yu et al. (2018) proposed a malyl-CoA-glycerate (MCG) pathway to augment the CBB cycle, which reduces energy requirements by 22.5% to produce the central metabolite, acetyl-CoA. Implementing the MCG pathway would thus have potential benefit to this study's IPA, but not the BDO, cell factory. More generally, Gleizer et al. (2019) were the first to introduce an entire CO_2 fixation pathway into a heterotrophic cell factory by relying on CBB cycle enzymes and formate assimilation. This significant achievement in metabolic engineering imparted chemolithotrophic metabolism to *E. coli*. Given formate needs to be oxidized to CO_2 at a molar ratio of ~8 [(mol formate)/(mol CO_2 fixed)] to provide reducing power for the CBB cycle, the carbon efficiency of this formate-assisted pathway is low and the cell's energy efficiency no better than the conventional CBB cycle. Furthermore, the production of formate from CO_2 via electrolysis is challenged by appreciable electricity demand and by electrode poisoning of the noble metal catalyst (Lee et al., 2019), where megawatt-scale implementation would be as capital intensive as for H_2O electrolysis (Schmidt et al., 2017). Despite their apparent thermodynamic promise, no artificial CO_2 fixation pathways have been successfully implemented in a cell factory. The problem of poor energy efficiency needs to be solved another way.

Low-cost renewable H_2 production is essential to achieving favorable techno-economics, although this is only part of the solution. Biomass pyrolysis-gasification needs to be implemented at considerable scale to justify the required solids handling capital investment, which may be mismatched with the more distributed

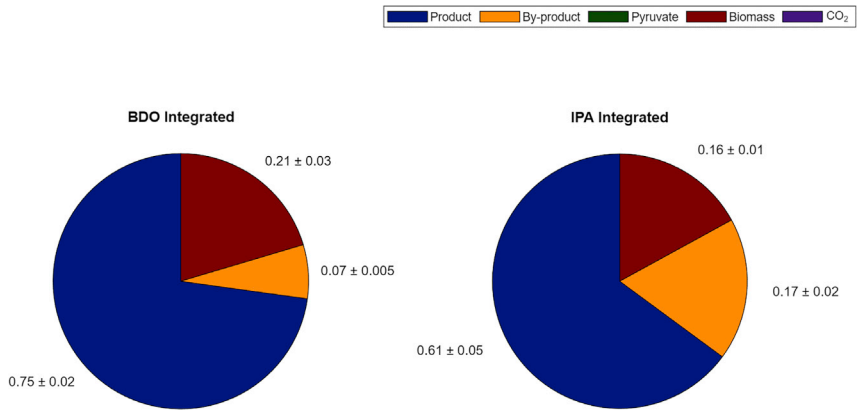

Figure 6. Molar Carbon Efficiencies for Continuous, Autotrophic Fermentations
Molar carbon efficiency (yield) of microbial cell factories in autotrophic fermentation, representing the carbon split using CO_2 as carbon source in [(C-mol product)/(C-mol CO_2)]. The by-product for the BDO strains is meso-2,3-butanediol and for the IPA strains is acetone. Table 2 summarizes additional performance parameters.

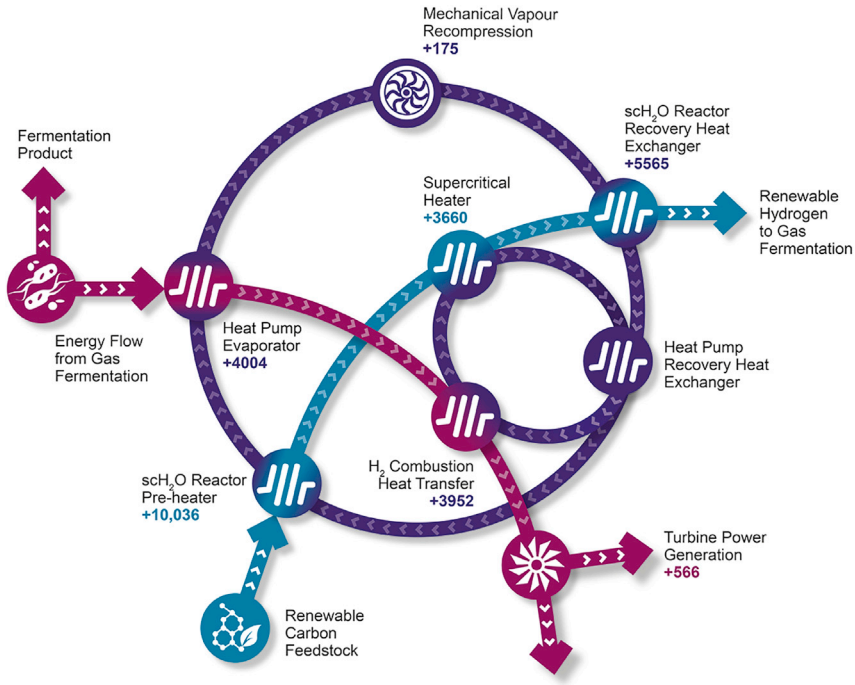

Figure 7. Schematic of the Heat Integration between Gas Fermentation and Supercritical Water Gasification
Schematic summarizing the heat integration between gas fermentation and supercritical water gasification via a heat pump using isopentane as enthalpy carrying fluid though a number of heat exchangers. The Heat Pump Evaporator recovers heat from the bioreactor at low temperature (4,004 kW/ton guaiacol), resulting in a reduction in the operating cost burden associated with cooling water use and electricity demand (see Figure 9). The cumulative recovery of heat energy within the heat pump cycle (purple cycle) minimizes the fraction of the H_2 (pink arc) that needs to be combusted to heat the aqueous guaiacol fed (blue arc) to the highly endothermic gasification reactor via the Supercritical Heater (3,660 kW/ton guaiacol).

nature of smaller bio-manufacturing facilities (Dou et al., 2019). Dark H_2 fermentation of complex carbohydrates suffers from low process intensification (Boboescu et al., 2016), whereas megawatt-scale H_2O electrolysis is too capital intensive making large-scale H_2 production prohibitive (Schmidt et al., 2017). Supercritical H_2O gasification needs to overcome corrosion and fouling challenges but can be implemented cost-effectively at a smaller scale, demonstrates high reaction rates, and is not prohibitive from a capital investment perspective (Okolie et al., 2019). Cost-effective catalysis is key to economically viable H_2 production at temperatures ~400°C, where scH_2O presents opportunities to produce nano-catalyst *in situ* (Huang et al., 2019) and for the recycle of valuable metals from spent catalyst (Grumett, 2003). Pertinent to this study, in addition to serving as a source of renewable H_2, the highly endothermic scH_2O gasification reaction provides a heat sink for the highly exothermic gas fermentation.

The consumption of H_2 to fuel the CBB cycle's kinetics generates a significant amount of heat at low temperature in bioreactors, which is conventionally removed via a chiller unit at the expense of electrical energy and high cooling water duty as shown in Figure 9. A heat pump can be employed to facilitate the energy (heat) flow from a low temperature (gas fermentation) to a high temperature (scH_2O gasification) via a thermal cycle as outlined in Figure 7 and detailed in Figure 8. Comparing the capital intensity of a conventional flowsheet (Figure 9) and the heat integrated flowsheet (Figure 8), Figure 8 has (1) a turbo-expander rather than a megawatt-scale air compressor, (2) a heat pump rather than a chiller thermal cycle, and (3) further energy recovery via a turbine. Reducing the operating cost burden associated with compression for gas fermentation, a turbo-expander supplies air for gas fermentation and the combustion chamber with no intrinsic electrical power consumption. In addition to producing 148 kg of BDO per ton of gasified guaiacol, comparable with guaiacol as sole carbon source (Figure 9), the process generates 566 kW of renewable electricity rather than consuming significant electrical power. From Figure 7, the overall heat duty of the scH_2O gasifier amounts to 13.7 MW/ton guaiacol. Without heat integration with gas fermentation, the combustion chamber would need to supply 58% of this heat duty, severely limiting the supply of H_2 per ton of guaiacol to gas fermentation, whereas with heat integration only 29% of this heat duty needs to be obtained by

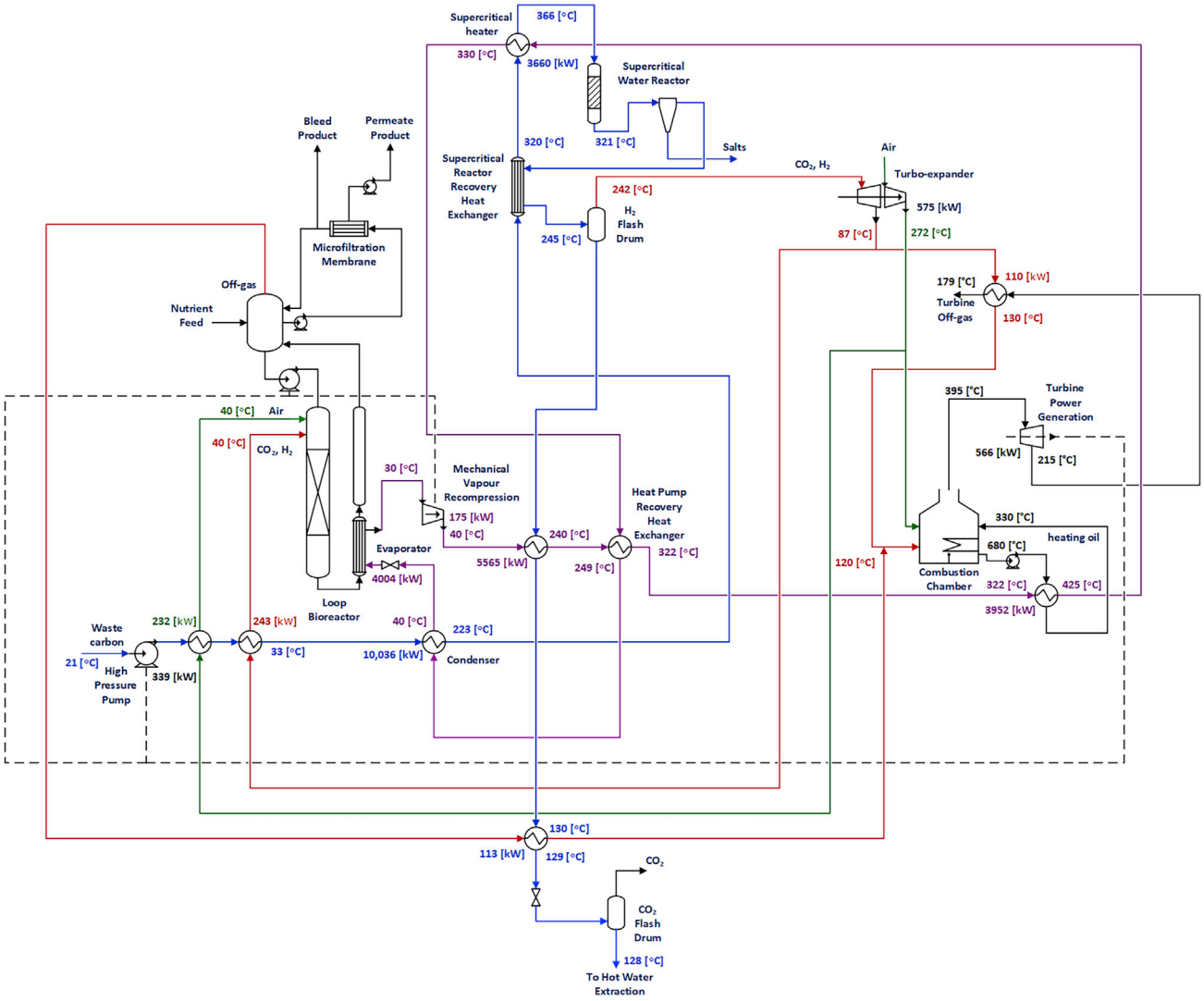

Figure 8. Process Flow Diagram for the Heat Integration between Gas Fermentation and Supercritical Water Gasification

Process flow diagram detailing the heat integration between gas fermentation and supercritical water gasification on a guaiacol feed basis of 1,000 kg/h. H_2-rich gas (red) is produced from waste carbon in the aqueous media (blue) in a scH_2O reactor. A heat pump using isopentane (purple) heat integrates the low-temperature gas fermentation with the high-temperature supercritical water gasifier through a number of heat exchangers. The H_2-rich product (red) from the supercritical H_2O gasification is feed to the gas fermentation and the combustion chamber as electron donor. Reducing the operating cost associated with compression for gas fermentation, the turbo-expander supplies air (green) with O_2 as electron acceptor for gas fermentation and the combustion chamber, respectively. In addition to producing 148 kg of BDO per ton of guaiacol, the process generates 566 kW of renewable electricity per ton of guaiacol with a negligible requirement for cooling water.

combusting a fraction of the gasifier's H_2 product. Recovering the heat generated to fuel the CBB cycle removes the thermodynamic inefficiency of CO_2 fixation as a significant burden to the process techno-economics. Although lignin is an abundant and low-cost feedstock, its recalcitrant, complex structure makes its direct exploitation in fermentation challenging. The process engineering solution in Figure 7 is not only energy efficient but also provides an innovative solution via scH_2O gasification to using renewable feedstocks such as lignin to produce chemicals. This study unlocks the promise of sustainable manufacturing using renewable feedstocks by combining the carbon efficiency of bio-catalysis with energy efficiency enforced through process engineering.

Limitations of the Study

In the design of a sustainable bio-manufacturing facility, capital cost is directly proportional to the productivity in the bioreactors, which impacts significantly on achieving favorable techno-economics. Although

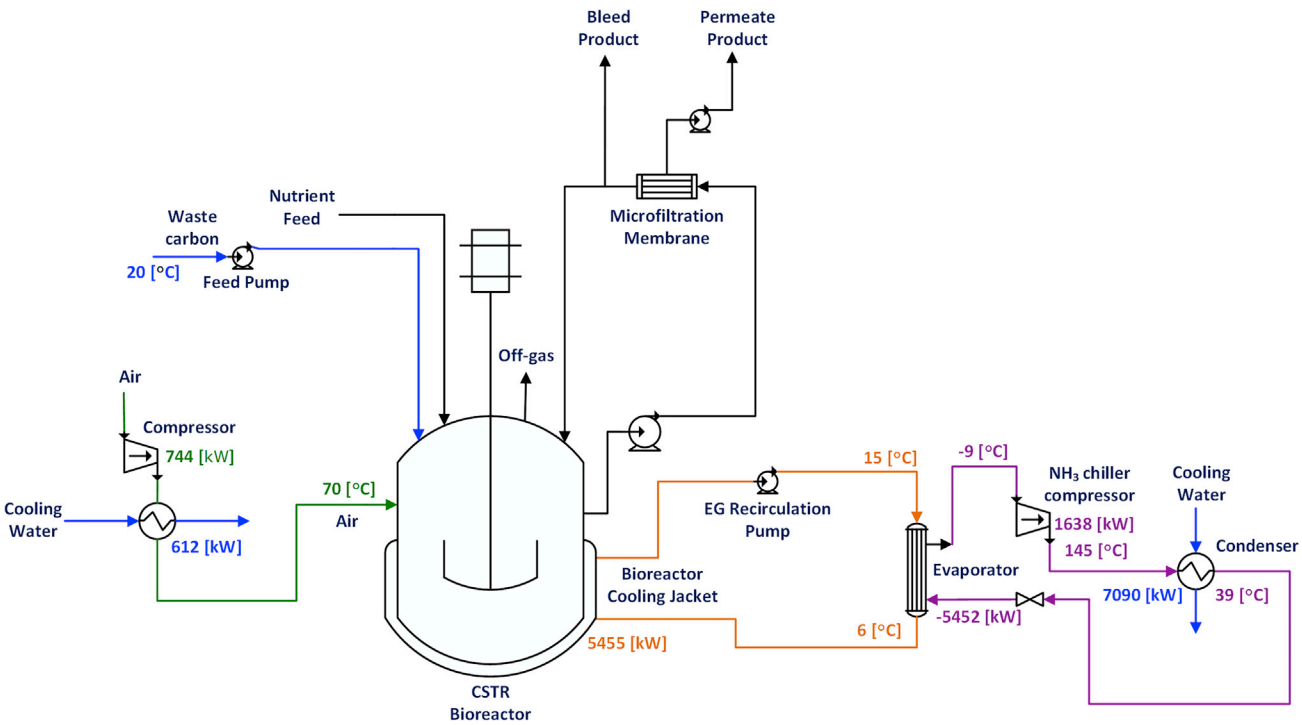

Figure 9. Process Flow Diagram for Conventional, Heterotrophic Fermentation of Guaiacol to BDO

Process flow diagram for waste carbon as sole energy and carbon source, modeled on a guaiacol feed basis of 1,000 kg/h. A chilled ethylene glycol (EG, orange) loop provides for heat removal from the bioreactor via an ammonia refrigeration unit (purple). The compressor and cooling water duties reflect the operating cost burden associated with this conventional heterotrophic operating strategy, producing 158 kg of BDO per ton of guaiacol.

this work is the first to demonstrate the stable and continuous bio-manufacture of chemicals from CO_2 using *C. necator* as a carbon-efficient cell factory, productivity in gas fermentation will be limited by O_2 transfer constraints in light of H_2 flammability. Therefore, process intensification toward higher O_2 mass transfer remains an important continued area of research. Although this study demonstrated stable and continuous gas fermentation experimentally, the integration of gas fermentation with scH_2O gasification was verified through process simulation. Notably, process simulators, such as Aspen HYSYS, provide for rigorous simulation that enables effective process design. Although this study is the first to demonstrate the use of process engineering to overcome the techno-economic hurdle associated with the energy inefficiency of biological CO_2 fixation, this work will benefit from the future demonstration of this integrated, continuous process at large laboratory scale.

Resource Availability

Lead Contact

Further information and requests for resources and reagents should be directed to and will be fulfilled by the Lead Contact, Rajesh Reddy Bommareddy (rajesh.bommareddy@nottingham.ac.uk).

Materials Availability

Materials generated in this study are available from the Lead Contact under Material Transfer Agreement (MTA).

Data and Code Availability

The ScrumPy package of metabolic modeling tools (build OMICS_20,375) was used for all systems biology simulations (Poolman, 2006). Aspen HYSYS V11 (build 37.0.0.395) from Aspen Technologies, Inc. was used for all process simulations in this study. Experimental sensor and analytical data from shake flask and continuous fermentation experiments (please see Transparent Methods section) were processed in Microsoft Excel 2016. Graphical representations of the processed data were produced using MATLAB R2019b

(9.7.0) version 19.0 from Mathworks, Incorporated. Data and code generated in this study are available from the Lead Contact under MTA.

METHODS

All methods can be found in the accompanying Transparent Methods supplemental file.

SUPPLEMENTAL INFORMATION

Supplemental Information can be found online at https://doi.org/10.1016/j.isci.2020.101218.

ACKNOWLEDGMENTS

This work was supported by the Biotechnology and Biological Sciences Research Council (BBSRC, Grant numbers BB/L013940/1 & BB/N023773/1) and the Engineering and Physical Sciences Research Council (EPSRC, Grant numbers BB/L013940/1 & BB/N023773/1). Also, the authors gratefully acknowledge support received from the University of Nottingham Research Beacon of Excellence: Green Chemicals. At the University of Nottingham, the authors gratefully acknowledge Mr. Matthew Abbott for undertaking the HPLC analyses; Dr. Naglis Malys and Mr. Joshua Gascoyne for support with the synthetic biology methods; and Dr. Jamie Twycross for his support with the metabolic modeling-based computational methods. At Johnson Matthey, the authors gratefully acknowledge the insightful contributions from Darren Gobby and David Watson.

AUTHOR CONTRIBUTIONS

Conceptualization: R.R.B., E.L., A.V.C.; Methodology: R.R.B., Y.W., and A.V.C; Software: Y.W., N.P., and A.V.C.; Formal Analysis: R.R.B., N.P., and A.V.C; Investigation: R.R.B., Y.W., N.P., and A.V.C.; Writing – Original Draft: R.R.B and A.V.C.; Writing – Review & Editing: R.R.B., Y.W., N.P., M.H., N.P.M., E.L., and A.V.C.; Visualization: R.R.B, Y.W., and A.V.C.; Supervision: A.V.C.; Funding Acquisition: N.P.M. and A.V.C.

DECLARATION OF INTERESTS

The authors declare no competing interests.

Received: March 3, 2020
Revised: May 7, 2020
Accepted: May 28, 2020
Published: June 26, 2020

REFERENCES

Axon, S., and James, D. (2018). The UN Sustainable Development Goals: how can sustainable chemistry contribute? A view from the chemical industry. Curr. Opin. Green Sustain. Chem. *13*, 140–145.

Bar-Even, A., Flamholz, A., Noor, E., and Milo, R. (2012). Thermodynamic constraints shape the structure of carbon fixation pathways. Biochim. Biophys. Acta *1817*, 1646–1659.

Boboescu, I.Z., Gherman, V.D., Lakatos, G., Pap, B., Bíró, T., and Maróti, G. (2016). Surpassing the current limitations of biohydrogen production systems: the case for a novel hybrid approach. Bioresour. Technol. *204*, 192–201.

Brigham, C. (2019). Perspectives for the biotechnological production of biofuels from CO2 and H2 using *Ralstonia eutropha* and other 'Knallgas' bacteria. Appl. Microbiol. Biotechnol. *103*, 2113–2120.

Brigham, C.J., Gai, C.S., Lu, J., Speth, D.R., Worden, R.M., and Sinskey, A.J. (2013). Engineering *Ralstonia eutropha* for production of isobutanol from CO2, H2, and O2. In Advanced Biofuels and Bioproducts (Springer), pp. 1065–1090.

Dou, B., Zhang, H., Song, Y., Zhao, L., Jiang, B., He, M., Ruan, C., Chen, H., and Xu, Y. (2019). Hydrogen production from the thermochemical conversion of biomass: issues and challenges. Sustain. Energy Fuels *3*, 314–342.

Emerson, D.F., and Stephanopoulos, G. (2019). Limitations in converting waste gases to fuels and chemicals. Curr. Opin. Biotechnol. *59*, 39–45.

Fründ, C., Priefert, H., Steinbüchel, A., and Schlegel, H.G. (1989). Biochemical and genetic analyses of acetoin catabolism in *Alcaligenes eutrophus*. J Bacteriol. *171*, 6539–6548.

Gleizer, S., Ben-Nissan, R., BAR-On, Y.M., Antonovsky, N., Noor, E., Zohar, Y., Jona, G., Krieger, E., Shamshoum, M., Bar-Even, A., and Milo, R. (2019). Conversion of *Escherichia coli* to generate all biomass carbon from CO2. Cell *179*, 1255–1263.e12.

Gruber, S., Hagen, J., Schwab, H., and Koefinger, P. (2014). Versatile and stable vectors for efficient gene expression in *Ralstonia eutropha* H16. J. Biotechnol. *186*, 74–82.

Grumett, P. (2003). Precious metal recovery from spent catalysts. Platinum Met. Rev. *47*, 163–166.

Hedstrom, L. (2010). Enzyme Specificity and Selectivity (eLS).

Hoffmeister, S., Gerdom, M., Bengelsdorf, F.R., Linder, S., Flüchter, S., Öztürk, H., Blümke, W., May, A., Fischer, R.J., Bahl, H., and Dürre, P. (2016). Acetone production with metabolically engineered strains of *Acetobacterium woodii*. Metab. Eng. *36*, 37–47.

Huang, J., Zhu, C., Lian, X., Feng, H., Sun, J., Wang, L., and Jin, H. (2019). Catalytic supercritical water gasification of glucose with in-situ generated nickel nanoparticles for hydrogen production. Int. J. Hydrogen Energy *44*, 21020–21029.

Ji, X.J., Huang, H., and Ouyang, P.K. (2011). Microbial 2,3-butanediol production: a state-of-the-art review. Biotechnol. Adv. *29*, 351–364.

Keijer, T., Bakker, V., and Slootweg, J.C. (2019). Circular chemistry to enable a circular economy. Nat. Chem. *11*, 190–195.

Krieg, T., Sydow, A., Faust, S., Huth, I., and Holtmann, D. (2018). CO(2) to terpenes: autotrophic and electroautotrophic α-humulene production with *Cupriavidus necator*. Angew. Chem. Int. Ed. *57*, 1879–1882.

Lee, C.W., Cho, N.H., Nam, K.T., Hwang, Y.J., and Min, B.K. (2019). Cyclic two-step electrolysis for stable electrochemical conversion of carbon dioxide to formate. Nat. Commun. *10*, 3919.

Li, H., Opgenorth, P.H., Wernick, D.G., Rogers, S., Wu, T.Y., Higashide, W., Malati, P., Huo, Y.X., Cho, K.M., and Liao, J.C. (2012). Integrated electromicrobial conversion of CO2 to higher alcohols. Science *335*, 1596.

Mallinson, S.J.B., Machovina, M.M., Silveira, R.L., Garcia-Borràs, M., Gallup, N., Johnson, C.W., Allen, M.D., Skaf, M.S., Crowley, M.F., Neidle, E.L., et al. (2018). A promiscuous cytochrome P450 aromatic O-demethylase for lignin bioconversion. Nat. Commun. *9*, 2487.

Marc, J., Grousseau, E., Lombard, E., Sinskey, A.J., Gorret, N., and Guillouet, S.E. (2017). Over expression of GroESL in *Cupriavidus necator* for heterotrophic and autotrophic isopropanol production. Metab. Eng. *42*, 74–84.

Molitor, B., Marcellin, E., and Angenent, L.T. (2017). Overcoming the energetic limitations of syngas fermentation. Curr. Opin. Chem. Biol. *41*, 84–92.

Müller, J., Maceachran, D., Burd, H., Sathitsuksanoh, N., Bi, C., Yeh, Y.C., Lee, T.S., Hillson, N.J., Chhabra, S.R., Singer, S.W., and Beller, H.R. (2013). Engineering of *Ralstonia eutropha* H16 for autotrophic and heterotrophic production of methyl ketones. Appl. Environ. Microbiol. *79*, 4433–4439.

Okolie, J.A., Rana, R., Nanda, S., Dalai, A.K., and Kozinski, J.A. (2019). Supercritical water gasification of biomass: a state-of-the-art review of process parameters, reaction mechanisms and catalysis. Sustain. Energy Fuels *3*, 578–598.

Park, J.M., Kim, T.Y., and Lee, S.Y. (2011). Genome-scale reconstruction and in silico analysis of the *Ralstonia eutropha* H16 for polyhydroxyalkanoate synthesis, lithoautotrophic growth, and 2-methyl citric acid production. BMC Syst. Biol. *5*, 101.

Peplinski, K., Ehrenreich, A., Döring, C., Bömeke, M., Reinecke, F., Hutmacher, C., and Steinbüchel, A. (2010). Genome-wide transcriptome analyses of the 'Knallgas' bacterium *Ralstonia eutropha* H16 with regard to polyhydroxyalkanoate metabolism. Microbiology *156*, 2136–2152.

Poolman, M.G. (2006). ScrumPy: metabolic modelling with Python. Syst. Biol. (Stevenage) *153*, 375–378.

Przybylski, D., Rohwerder, T., Harms, H., and Mueller, R.H. (2012). Third-generation feed stocks for the clean and sustainable biotechnological production of bulk chemicals: synthesis of 2-hydroxyisobutyric acid. Energ. Sustain. Soc. *2*, 11.

Raberg, M., Voigt, B., Hecker, M., and Steinbüchel, A. (2014). A closer look on the polyhydroxybutyrate- (PHB-) negative phenotype of *Ralstonia eutropha* PHB-4. PLoS One *9*, e95907.

Rodriguez Correa, C., and Kruse, A. (2018). Supercritical water gasification of biomass for hydrogen production – Review. J. Supercrit. Fluids *133*, 573–590.

Schmidt, O., Gambhir, A., Staffell, I., Hawkes, A., Nelson, J., and Few, S. (2017). Future cost and performance of water electrolysis: an expert elicitation study. Int. J. Hydrogen Energy *42*, 30470–30492.

Shen, X., Meng, Q., Mei, Q., Liu, H., Yan, J., Song, J., Tan, D., Chen, B., Zhang, Z., Yang, G., and Han, B. (2020). Selective catalytic transformation of lignin with guaiacol as the only liquid product. Chem. Sci. *11*, 1347–1352.

Steinbüchel, A., and Schlegel, H.G. (1989). Excretion of pyruvate by mutants of *Alcaligenes eutrophus*, which are impaired in the accumulation of poly(β-hydroxybutyric acid) (PHB), under conditions permitting synthesis of PHB. Appl. Microbiol. Biotechnol. *31*, 168–175.

Tanaka, K., Ishizaki, A., Kanamaru, T., and Kawano, T. (1995). Production of poly(D-3-hydroxybutyrate) from CO(2), H(2), and O(2) by high cell density autotrophic cultivation of *Alcaligenes eutrophus*. Biotechnol. Bioeng. *45*, 268–275.

Tian, P., Wei, Y., Ye, M., and Liu, Z. (2015). Methanol to olefins (MTO): from fundamentals to commercialization. ACS Catal. *5*, 1922–1938.

Toyir, J., Miloua, R., Elkadri, N.E., Nawdali, M., Toufik, H., Miloua, F., and Saito, M. (2009). Sustainable process for the production of methanol from CO2 and H2 using Cu/ZnO-based multicomponent catalyst. Phys. Proced. *2*, 1075–1079.

Tudor, R., and Shah, A. (2017). Industrial low pressure hydroformylation: forty-five years of progress for the LP OxoSM process. Johnson Matthey Technol. Rev. *61*, 246–256.

Voss, I., and Steinbüchel, A. (2006). Application of a KDPG-aldolase gene-dependent addiction system for enhanced production of cyanophycin in *Ralstonia eutropha* strain H16. Metab. Eng. *8*, 66–78.

Wang, W., Yang, S., Hunsinger, G.B., Pienkos, P.T., and Johnson, D.K. (2014). Connecting lignin-degradation pathway with pre-treatment inhibitor sensitivity of *Cupriavidus necator*. Front. Microbiol. *5*, 247.

Windhorst, C., and Gescher, J. (2019). Efficient biochemical production of acetoin from carbon dioxide using *Cupriavidus necator* H16. Biotechnol. Biofuels *12*, 163.

Yu, H., Li, X., Duchoud, F., Chuang, D.S., and Liao, J.C. (2018). Augmenting the Calvin–Benson–Bassham cycle by a synthetic malyl-CoA-glycerate carbon fixation pathway. Nat. Commun. *9*, 2008.

iScience, Volume *23*

Supplemental Information

A Sustainable Chemicals Manufacturing Paradigm Using CO_2 and Renewable H_2

Rajesh Reddy Bommareddy, Yanming Wang, Nicole Pearcy, Martin Hayes, Edward Lester, Nigel P. Minton, and Alex V. Conradie

SUPPLEMENTAL INFORMATION

TRANSPARENT METHODS

METABOLIC ENGINEERING

Gene selection

The biochemical network for the synthesis of BDO and IPA in the microbial cell factory, *C. necator* H16, is outlined in Figure 1A. The BDO biochemical pathway entails three enzymatic steps from pyruvate, where pyruvate is converted to 2-acetolactate by the feedback resistant *2-acetolactate synthase* from *Bacillus subtilis* (ALS, *alsS*). Thereafter, 2-acetolactate is decarboxylated to stereospecific (R)-acetoin by *acetolactate decarboxylase* from *Bacillus subtilis* (ALDC, *alsD*). Finally, (R)-acetoin is reduced to BDO by a NADPH-specific *secondary alcohol dehydrogenase* (sADH, *adh*) from *Clostridium beijerinckii*. The isopropanol (IPA) pathway entails a four-step enzymatic conversion of two moles of acetyl-CoA to one mole of IPA (Figure 1A). Acetyl-CoA is converted to acetoacetyl-CoA by a *β-ketothiolase* from *C. necator* (*phaA*). Thereafter, acetoacetyl-CoA is hydrolysed to acetoacetate by a *CoA-transferase* from *Helicobacter pylori* (ctfAB, c*tfAB*) and decarboxylated to acetone by a decarboxylase from *Clostridium acetobutylicum* (ADC, *adc*). Finally, acetone is reduced to IPA by a NADPH-dependent *secondary alcohol dehydrogenase* from *Clostridium beijerinckii* (sADH, *adh*). The genes encoding for the enzymes of the BDO and IPA pathways are detailed in Table S4.

Synthetic biology

Growth media and heterotrophic cultures

Unless stated otherwise, lysogeny broth (LB) was used for routine cultivations of *E.coli* and *C. necator*, adding 15 [g/L] agar for solid media plates. Where required, antibiotic selection pressure at 300 [µg/mL] and 50 [µg/mL] kanamycin (kan^r) was used for *C. necator* and *E.coli* cultures respectively. For pLO3 vector based cultivations, 12.5 [µg/mL] tetracycline (Tc^r) was used for *E.coli* and *C. necator*. Shake flask cultivations were performed in 500mL baffled flasks with 50 [mL] working volume and incubated at 30 [°C] and 200 [rpm]. The minimum media recipe advocated by (Schlegel et al., 1961) was used for all microbial shake flask performance evaluations including 20 [g/L] fructose as carbon source. Shake flask evaluations were incubated for 72 [h].

Plasmid cloning & transformation protocols

The genetic constructs for the BDO and IPA pathways were codon optimised for expression in *C. necator* and synthetised using Invitrogen Geneart® gene synthesis (Table S5). All primers used in the study are listed in Table S1. DNA amplification was performed using Phusion U hot start

39 polymerase (NEB) with GC buffer for USER assembly. GC rich DNA amplifications were performed
40 using Phusion polymerase with green GC buffer (NEB). For routine DNA amplifications, DreamTaq
41 polymerase master mix (Thermo Scientific) was used. The pBAD promoter with the *araC* gene was
42 obtained from the plasmid, pCM291rfp. Ribosome binding sites (RBS) were taken from previous
43 studies as outlined in Table S2. Plasmids (see Table S3) were constructed with USER assembly kit
44 (New England Biolabs, NEB) and transformed into *E.coli* DH5α by heat-shock method. The
45 plasmids were extracted using mini-prep kit from NEB (Monarch®) and transformed into *C. necator*
46 by electroporation using a 0.2cm cuvette (Bio-rad), at 2.5 kV, 200Ω and 25μF using a GenePulser®
47 electroporation unit (Ausubel, 2003).
48
49 ***Chromosomal attenuation and integration protocol***
50 For chromosomal attenuation and integration, suicide vectors (see Table S3) were transformed via
51 conjugation using *E.coli* S-17 cells carrying the desired vector and *C. necator* strains using the
52 protocol described by Lenz et al (Lenz and Friedrich, 1998). Suicide vectors (pLO3 based) with
53 flanking regions were created by overlap extension PCR using primers listed in Table S1. The BDO
54 operon was placed between 750bp homology arms, each flanking upstream of *phaC1*'s start codon
55 and downstream of *phaB1*'s stop codon, producing a suicide vector pLO3-CAB-BD-2 (Table S3).
56 This vector was then used to knock-out the *phaC1AB1* operon in H16 and knock-in the BDO operon,
57 creating the strain H16-CAB-BD2. The IPA operon was placed between 750bp homology arms each
58 flanking 750bp upstream of *phaC1* start codon and *phaC1* stop codon producing vector pLO3-CB-
59 IPA4. This vector was used to attenuate *phaC1* in the H16-B strain (knockout of *phaB1*) and knock-
60 in the IPA operon upstream of *phaA* gene. Trans-conjugants were selected on minimal media plates
61 with 0.4 [%] (w/w) fructose and appropriate antibiotics. Knock-in and knock-off events for
62 integrating the operons were performed by two-step homologous recombination (tet^r and *sacB*
63 selection). The first recombination event, i.e. the first crossover, was confirmed on LB plates using
64 tetracycline as the selection marker. The second recombination step was carried out by inoculating
65 single colonies from the first crossover into low salt LB medium with 15 [%] (w/v) sucrose without
66 antibiotics overnight. Sucrose resistant colonies were plated on low salt LB agar plate with 15 [%]
67 (w/v) sucrose, and single colonies were selected for further screening. Colonies without antibiotic
68 resistance (tet^r) were selected and successful integration was confirmed via PCR using primers
69 flanking the upstream and downstream regions of the chosen homologous sequences. Integration
70 was also confirmed using Sanger sequencing (Eurofins genomics GmbH).
71
72 **GAS FERMENTATION**
73
74 ***Gas fermentation media***
75 Pre-cultures for bioreactor cultivations were prepared in tryptic soy broth (TSB) medium from a
76 single colony and incubated overnight at 200 [rpm], 30 [°C] in 500mL baffled flask with 100 [mL]

working volume. Modified DSMZ 81 medium was used for autotrophic bioreactor cultivations, where the vitamin solution and $NaVO_3$ were omitted. Metaphosphates were added instead of orthophosphates in the form of trisodium trimetaphosphate ($Na_3P_3O_9$) to avoid struvite precipitation. L-Arabinose was added at a final concentration of 1 [g/L] (0.1 [%] (w/v)) for culture induction.

Bioreactor setup

As depicted in Figure 3, continuous fermentations were performed in a DASGIP® bioreactor system (Eppendorf), using 1L capacity vessels with a 750 [mL] working volume, fitted with a headplate condenser chilled to 10 [°C]. The agitation system comprised two Rushton turbine impellers. Gas sparging was via two pin-hole, L-shaped spargers, separating the CO_2 and air feed from the H_2 feed. For continuous operation, the level in the bioreactor vessel was controlled (LIC100) using a conductivity probe positioned at an appropriate height in the vessel. The temperature was controlled (TIC100) at 30 [°C] using a chilled water feed. The pH was monitored by a Mettler Toledo pH probe, calibrated at pH = 4 and pH =7 in standard pH buffers. The pH was controlled (AIC100) at a set point of 6.9 using 5 [%] (w/v) NH_3(aq). The dissolved oxygen (DO) concentration was monitored using an optical Mettler Toledo DO probe, calibrated *in situ* at atmospheric pressure in N_2 at 0 [%] pO_2 and in air at 100 [%] pO_2. The DO was controlled (AIC101) at micro-aerobic, steady state concentration through phosphate addition under phosphate limiting conditions. The off-gas outlet from the bioreactor was fed to an external foam trap bottle, fitted with an optical oxygen probe (VisiFerm, Hamilton), calibrated at 0 [%] (v/v) with N_2 and at 10 [%] (v/v) with 10 [%] (v/v) O_2 in N_2. The off-gas O_2 concentration was controlled (AIC102) at a non-flammable set point of 4 [%] (v/v) by controlling the air flow rate (FIC100) to the bioreactor. Guarding against a flammable atmosphere, a safety trip was programmed into the Dasware® software, which interlocked all the gases feeds should the off-gas O_2 concentration rise above 5 [%] (v/v), flooding the bioreactor with N_2.

The initial agitation speed (SIC100) was set at 400 [rpm] and stepped to a maximum agitation of 1600 [rpm] approximately 24 [h] after inoculation. CO_2 was fed via a mass flow controller (FIC101) at a rate of 1.35 [L/h]. H_2 was fed via mass flow controller (FIC102) at a rate of 35.1 [L/h]. The mass flow rates for CO_2, H_2 and Air mass flow controllers were calibrated using a M13 mini CORI-FLOW Coriolis Mass Flow Meter from Bronkhorst, ranged between 0 – 50 [g/h]. The Nutrient Feed media, containing 0.1 [%] (w/w) arabinose as inducer, was fed at 7 [mL/h] via a peristaltic pump. The off-gas from the external foam trap bottle was connected to a local exhaust ventilation (LEV) unit and the whole bioreactor setup was placed in the LEV with polycarbonate doors to ensure a ventilated enclosure.

115 **ANALYTICAL METHODS**
116
117 ***Liquid fraction analyses***
118 Supernatants from the shake flask and fermentation cultivations were obtained by centrifuging
119 culture samples for 5 [min] at 13000 [rpm]. Fructose, pyruvate, acetoin, meso-2,3-butanediol, R,R-
120 2,3-butanediol, S,S-2,3-butanediol, acetone, acetate, succinate and isopropanol were analysed
121 using an HPLC with an Aminex HPX-87H column (Bio-Rad, Hercules, CA), equipped with UV and RI
122 detectors. The flow rate of the 5 [mM] H_2SO_4 mobile phase was set at an isocratic 0.5 [mL/min] with
123 a column temperature of 50 [°C]. Quantifications were performed from the standard curves
124 obtained using standards purchased from Sigma Aldrich.
125
126 Dry cell weight (DCW) measurement was used as primary method for biomass concentration. DCW
127 was determined by centrifuging 1 [mL] culture in a pre-weighted 2mL Eppendorf tube. After
128 washing once with distilled water, the pellet was dried for 48 [h] at 100 [°C] and weighed. Optical
129 density measurement was used as secondary method for biomass concentration, quantified using
130 a spectrophotometer at an optical density of 600 [nm]. A correlation factor of 1 OD600 = 0.30 ± 0.03
131 [g/L] biomass was determined with an R^2 = 0.96.
132
133 ***Gas fraction analyses***
134 Off-gas analyses from fermentation were undertaken in-line after the foam trap using a
135 multiplexed Raman Laser Analyzer from Atmospheric Recovery Incorporated. The span for the off-
136 gas analyser was calibrated with two high specification gas mixtures from BOC Gases, containing
137 ultra-high purity (UHP) argon as the background gas. The two gas mixtures were (1) 40 [%] (v/v) H_2
138 in UHP argon, and (2) 4 [%] (v/v) O_2, 50 [%] (v/v) N_2 and 3 [%] (v/v) CO_2 in UHP argon. The zero
139 calibration was undertaken in UHP purity argon. The off-gas analyser was set to sample for 20 [s]
140 from each fermenter in an 80 [s] cycle at a sample flow rate of 280 [mL/min].
141
142 **SYSTEMS BIOLOGY AND PROCESS SIMULATION**
143
144 ***Systems Biology biochemical network simulation***
145 The ScrumPy metabolic modelling software package (Poolman, 2006) was used to simulate carbon
146 fluxes using a genome scale model for *C. necator* (Unpublished Data), which advances on the
147 existing model proposed by Park et al (Park et al., 2011). The cell's ATP maintenance requirement
148 for autotrophic growth was set at 10 [mmol/(gDCW·h)] and 3 [mmol/(gDCW·h)] for heterotrophic
149 growth. The BDO pathway genes were added to the genome scale model for wild-type *C. necator*
150 H16 as per Figure 1A. For the simulations using guaiacol as sole energy and carbon source, the
151 cytochrome P450 aromatic *O-demethylase* characterised by Mallinson et al (Mallinson et al., 2018)
152 was incorporated into the genome scale model. Carbon uptake rates for the carbon source, either

CO_2 or guaiacol, and biomass growth rates were constrained to align with fermentation data. The objective function for Flux Balance Analysis (FBA) was to maximise the BDO production in light of the overexpressed BDO pathway.

Aspen HYSYS process simulations

The process simulator, ASPEN HYSYS V11, was used to rigorously model the heat integration of gas fermentation with scH_2O gasification through a heat pump thermal cycle. The Lee-Kesler-Plocker equation of state was used to model the thermodynamic properties of the process fluids, given it represents the most accurate enthalpy model for high pressure gases. The scH_2O gasification reactor was modelled as a plug flow reactor using the pseudo first order, Ni-catalysed kinetic rate constant proposed by DiLeo et al (DiLeo et al., 2007). The bioreactor was modelled as a conversion reactor using the experimentally determined reaction stoichiometry for CO_2 & H_2 and the FBA simulation stoichiometry for the guaiacol bioreactor. Similarly, the combustion chamber was modelled as a conversion reactor, assuming total conversion of the H_2 and O_2 to H_2O. Compressors were modelled having a single stage with an adiabatic efficiency of 75 [%]. Turbines were modelled as having an isentropic efficiency of 75 [%]. Heat exchangers were modelled as single pass shell-and-tube, maintaining a minimum approach temperature of 10 [°C]. Given the high accuracy of the Lee-Kesler-Plocker equation of state, ASPEN HYSYS was also employed to estimate the volatile product fraction for the BDO and IPA continuous gas fermentations.

Table S1. Sequences of primers. Related to Figure 1B.

Primer	**Sequence (5′ ----> 3′)**
U-ara-F	gggaaagUaacgttatgacaacttgacggctac
U-ara-R	atatctccUtcttaaaagatcttttgaattccc
U-alsS-F	aggagataUacatatgaccaaggccaccaaggaacag
U-alsS-R	atggtaacUtctcctttacgtacgtcacagcgccttggtcttcatcagc
U-alsD-F	agttaccaUgaagcgcgagtcgaacatccag
U-alsD-R	atggttgUcctcctttctcgagtcattccggcgagccctcg
U-sADH-F	acaaccaUgaagggcttcgccatgctg
U-sADH-R	ggagacaUcctaggtcacaggatcaccacggccttg
acoXABC-F	tgcccaacagcttctccggc
acoXABC-R	tcgcagaaggaaccggccac
Aco-up-sacI-F	ttatgagctctactaccgcctcaacggcgcg
Aco-dn-xbaI-R	ttattctagaggctcaggttgaggatgccg
Aco-ov-speI-F	ggagacaggcaatggggcacactagtcatctgggcggctgatgcc
Aco-ov-speI-R	ggcatcagccgcccagatgactagtgtgccccattgcctgtctcc
phaC-up-F	acgcgccgatgaacaggtc
phaB-dn-R	tgctcatcatgccctgcatcatcg
phaC-up-sacI-F	ttattgagctcacgccggtcgcttctactcctatc
phaB-dn-pacI-R	attatattaattaatcgatgtagttgctcatcatgccctg
phaCB-ov-speI-F	acggcagagagacaatcaaatcactagtcctaggcctgccggcctggttcaaccag
phaCB-ov-speI-R	ctggttgaaccaggccggcaggcctaggactagtgatttgattgtctctctgccgt
U-ctfAB-F	aggagataUacatatgaacaaggtgatcacggacc
U-ctfAB-R	atggtaacUtctcctttacgtacgtcacagatgcacctcgaactcg
U-adc-F	agttaccaUgctgaaggacgaggtgatc
U-adc-R	atggttgUcctcctttggatcctcacttcagatagtcgtagatcacttcgg
phaC-dn- pacI-R	attatattaattaaaaggcgggcttgaggccggac
phaC-dn-R	tctccatcaggtccaggtcttg
phaC-ov-speI-F	ggcagagagacaatcaaatcatggcgactagtaaggcatgacgcttgcatgagtgc
phaC-ov-speI-R	gcactcatgcaagcgtcatgccttactagtcgccatgatttgattgtctctctgcc
phaB1-up-sacI-F	ttattgagctccatcacacgcgaggc
phaB1-dn-xbaI-R	attattctagagcctggatgttcttttccag
phaB1-ov-speI-F	acgaagccaatcaaggagtggacactagtcctgccggcctggttc
phaB1-ov-speI-R	gaaccaggccggcaggactagtgtccactccttgattggcttcgt
phaB1-up-F	tcaagccggagcaggtgagc

198 **Table S2.** Ribosome binding sites. Related to Figure 1B.

RBS	***RBS sequence***	***Reference***
RBS1	*tttaagaaggagatatacatATG*	(Bi et al., 2013)
RBS2	*cgtacgtaaaggagaagttaccATG*	(Li and Liao, 2013)
RBS3	*aaaggaggacaaccATG*	(Grousseau et al., 2014)

199

200 **Table S3.** Strains and plasmids used in this study. Related to Figure 2.

***Cupriavidus necator* strains**	**Genotype or description**	**Reference or source**
H16	wild-type	DSM 428, ATCC 17699
H16-CAB	H16 with in-frame deletion of *phaC1AB1* operon	This study
H16-CAB-Aco	H16 with in-frame deletion of *phaC1AB1* and *acoXABC* operons	This study
H16-CAB-Aco-BD-2	CAB-Aco with integrated 2,3-BDO operon with NADPH-dependent alcohol dehydrogenase	This study
H16-CAB-Aco-p-BD-2	CAB-Aco with plasmid pBBR-BD-2	This study
H16-CB-IPA-4	H16-CB with integrated IPA-4 pathway	This study
H16-CB-p-IPA-4	H16-CB with pBBR-IPA-4	This study
H16-CB	H16 with in-frame deletion of *phaC1* and *phaB1*	This study
H16-B	H16 with in-frame deletion of *phaB1*	This study
***E.coli* strains**		
DH5α	*fhuA2 Δ(argF-lacZ)U169 phoA glnV44 Φ80 Δ(lacZ)M15 gyrA96 recA1*	Invitrogen
S17-1	*relA1 endA1 thi-1 hsdR17 recA pro hsdR RP4-2-Tc::Mu-Km::Tn7* integrated into the chromosome	Invitrogen
Plasmids		
pBBR1MCS-2-USER	Expression vector, Kan^r	(Alagesan et al., 2018)

***Cupriavidus necator* strains**	**Genotype or description**	**Reference or source**
pCM291rfp	Source of pBAD promoter with *araC* gene	(Bi et al., 2013)
pLO3	Suicide vector, Tc^r, *sacB*, RP4 ori, ColE1 ori	(Lenz and Friedrich, 1998)
pLO3-CB	pLO3 with 750 bp upstream region of *phaC1* and 750 bp downstream region of *phaB1*	This study
pLO3-C	pLO3 with 750 bp upstream region of *phaC1* and 750 bp downstream region of *phaC1*	This study
pLO3-B	pLO3 with 750 bp upstream region of *phaB1* and 750 bp downstream region of *phaB1*	This study
pBBR-BD-2	pBBR1MCS-2-USER with pBAD-ALS-ALDC-sADH	This study
pLO3-CAB-BD-2	pLO3 with 750 bp upstream region of *phaC1*-pBAD-ALS-ALDC-sADH and 750 bp downstream region of *phaB1*	This study
pLO3-acoXABC-KO	pLO3 with 850 bp upstream region of *acoX* and 900 bp downstream region of *acoC*	This study
pBBR-IPA-4	pBBR1MCS-2-USER with pBAD-ctfAB-ADC-sADH	This study
pLO3-C-IPA-4	pLO3 with 750bp upstream of *phaC*-pBAD-ctfAB-ADC-sADH and 750bp downstream region of *phaC1*	This study

201

202 **Table S4.** Pathway gene selection. Related to Figure 1B.

Pathway	**Gene**	***Enzyme***	***Host Origin***	***Accession number***	***Reference***
BDO pathway genes	*alsS*	2-acetolactate synthase	*Bacillus subtilis*	EnsemblBacteria: BSU36010	(Yan et al., 2009)
	alsD	acetolactate decarboxylase	*Bacillus subtilis*	EnsemblBacteria: BSU36000	(Yan et al., 2009)
	adh	NADPH-specific secondary alcohol dehydrogenase	*Clostridium beijerinckii*	GenBank: AAA23199.2	(Yan et al., 2009)

IPA pathway genes	*ctfAB*	CoA-transferase	*Helicobacter pylori*	GenBank: AJ000086.1	(Corthésy-Theulaz et al., 1997)
	adc	acetoacetate decarboxylase	*Clostridium acetobutylicum*	EnsemblBacteria: CA_P0165	(Grousseau et al., 2014)
	adh	NADPH-specific secondary alcohol dehydrogenase	*Clostridium beijerinckii*	GenBank: AAA23199.2	(Yan et al., 2009)

Table S5. Condon optimised sequences. Related to Figure 1B.

Gene	Sequence
alsS	atgaccaaggccaccaaggaacagaagtcgctggtcaagaatcgcggcgccgaactggtggtggactgcctggtggaacagg gcgtgacccacgtgttcggcatcccgggcgccaagatcgacgccgtgttcgacgcgctgcaggacaagggccccgagatcatc gtggcccgccacgagcagaatgccgccttcatggcccaggcggtgggccgcctgaccggcaagccgggcgtcgtgctggtgac gagcggcccgggcgcgagcaacctggccaccggcctgctgaccgccaacaccgaaggcgacccggtggtggccctggccggc aacgtgatccgcgccgaccgcctgaagcgcacccatcagtcgctggacaatgccgcgctgttccagccgatcaccaagtactcg gtggaagtgcaggacgtgaagaacatcccggaagccgtgaccaacgccttccgcatcgcctcggccggccaggccggcgccgc cttcgtgtcgttcccgcaggacgtcgtgaacgaggtgaccaacaccaagaacgtgcgcgccgtggccgcgccgaagctgggcc ccgccgccgacgacgccatctcggccgcgatcgccaagatccagaccgccaagctgccggtggtgctggtcggcatgaagggc ggccggccggaagcgatcaaggccgtgcgcaagctgctgaagaaggtgcagctgccgttcgtggaaacctaccaggccgcgg gcaccctgtcgcgcgatctggaagatcagtacttcggccgcatcggcctgttccgcaaccagccgggcgacctgctgctggaaca ggcggatgtggtgctgaccatcggctacgacccgatcgagtacgaccccaagttctggaacatcaacggcgaccgcaccatcat ccacctggacgaaatcatcgccgacatcgaccacgcctaccagccggacctggaactgatcggcgacatcccgagcacgatcaa ccacatcgagcatgacgccgtgaaggtcgagttcgccgagcgcgagcagaagatcctgtcggacctgaagcagtacatgcacg agggcgaacaggtgccggccgactggaagtcggatcgcgcccatccgctggaaatcgtgaaggaactgcgcaacgccgtgga cgaccacgtgaccgtgacctgcgacatcggctcgcacgccatctggatgtcgcgctacttccgcagctacgagccgctgacgctg atgatcagcaacggcatgcagaccctgggcgtcgccctgccgtgggccatcggcgcctcgctggtgaagcccggcgaaaaggt ggtgtcggtgagcggcgatggcggcttcctgttctcggccatggaactggaaaccgccgtgcgcctgaaggccccgatcgtgca catcgtgtggaacgactcgacctacgacatggtggccttccagcagctgaagaagtacaaccgcacctcggccgtggacttcgg caacatcgacatcgtgaagtacgccgagtccttcggcgccacgggcctgcgcgtggaatcgccggaccagctggccgacgtgct gcgccagggcatgaacgcggaaggcccggtgatcatcgacgtgccggtggactactcggacaacatcaacctggcgtcggaca agctgcccaaggagttcggcgagctgatgaagaccaaggcgctgtga
alsD	atgaagcgcgagtcgaacatccaggtgctgtcgcgcggccagaaggaccagccggtcagccaaatctaccaggtgtcgaccat gacctcgctgctggacggcgtgtacgacggcgacttcgagctgtcggagatcccgaagtacggcgatttcggcatcggcacctt caacaagctggatggcgagctgatcggcttcgacggcgagttctaccgcctgcgctcggatggcaccgccacgccggtgcaga acggcgatcgcagcccgttctgctcgttcaccttcttcaccccggacatgacccacaagatcgacgccaagatgacccgcgagga cttcgagaaggaaatcaactcgatgctgccgtcgcgcaacctgttctacgccatccgcatcgacggcctgttcaagaaggtgcag acccgcaccgtggaactgcaggaaaagccctacgtcccgatggtggaagccgtcaagacccagccgatcttcaacttcgacaac gtgcgcggcaccatcgtgggcttcctgacgccggcctacgccaacggcatcgccgtgtcgggctaccatctgcacttcatcgacg

	aaggccgcaacagcggcggccacgtgttcgactacgtgctggaagattgcaccgtgaccatctcgcagaagatgaacatgaac ctgcgcctgccgaacaccgccgatttcttcaacgccaacctggacaacccggacttcgccaaggacatcgaaaccaccgagggc tcgccggaatga
adh	atgaagggcttcgccatgctgggcatcaacaagctgggctggatcgagaaggaacgcccggtggccggcagctacgatgccat cgtgcgcccgctggccgtgtcgccgtgcacctcggatatccacaccgtgttcgaaggcgccctgggcgaccgcaagaacatgat cctgggccacgaggccgtgggcgaagtggtggaagtgggcagcgaggtgaaggacttcaagcccggcgaccgcgtgatcgt gccgtgcacgaccccggactggcgctcgctggaagtgcaggccggcttccagcagcactcgaacggcatgctggccggctgga agttctcgaacttcaaggacggcgtgttcggcgagtacttccacgtgaacgacgccgacatgaacctggccatcctgccgaagg acatgccgctggaaaacgccgtgatgatcaccgacatgatgaccacgggcttccatggcgccgagctggccgacatccagatgg gctcgtcggtggtggtgatcggcatcggcgccgtgggcctgatgggcatcgccggcgccaagctgcgcggcgccggccgcatc atcggcgtgggctcgcgcccgatctgcgtggaagcggccaagttctatggcgccaccgacatcctgaactacaagaacggccac atcgtggaccaggtgatgaagctgaccaacggcaagggcgtcgaccgcgtcatcatggccggcggcggctcggaaaccctgtc gcaggccgtgagcatggtcaagcccggcggcatcatctcgaacatcaactaccacggctcgggcgacgccctgctgatcccgcg cgtggaatggggctgcggcatggcccacaagaccatcaagggcggcctgtgcccgggcggccggctgcgcgccgaaatgctg cgcgacatggtggtgtacaaccgcgtggacctgtcgaagctggtgacccacgtgtaccatggcttcgaccacatcgaagaggcc ctgctgctgatgaaggacaagcccaaggacctgatcaaggccgtggtgatcctgtga
ctfAB	atgaacaaggtgatcacggacctggacaaggccctgtcgaccctgaaggacggcgacaccatcctggtcggcggctttggcctg tgcggcatcccggaatacgccatcgactacatctacaagaagggcatcaaggacctgatcgtggtgtcgaacaactgcggcgtg gacgacttcggcctgggcatcctgctggaaaagaagcagatcaagaagatcatcgccagctacgtgggcgagaacaaaatctt cgagtcgcagatgctgaacggcgagatcgaggtggtgctgaccccgcagggcaccctggccgaaaatctgcgccccggcggc gcgggcatcccgcctactacaccccgaccggcgtgggcacgctgatcgcccagggcaaggaatcgcgcgagttcaacggcaa ggaatacatcctggaacgcgccatcaccggcgactacggcctgatcaaggcctacaagtcggacaccctgggcaacctggtgtt ccgcaagaccgcgcgcaacttcaacccgctgtgcgccatggccgccaaaatctgcgtggccgaggtggaagagatcgtgccgg cgggcgaactggacccggacgagatccatctgccgggcatctacgtgcagcatatctacaagggcgagaagttcgagaagcgc atcgaaaagatcaccacgcgctcggccaaatgagggaagccatcatcaagcgcgccgccaaggaactgaaggaaggcatgta cgtcaatctgggcatcggcctgccgacgctggtcgccaatgaggtgtcgggcatgaacatcgtgttccagtcggagaacggcct gctgggcatcggcgcgtatccgctggaaggctcggtggacgccgacctgatcaatgccggcaaggaaaccgtgacggtcgtcc cgggcgcctcgttcttcaactcggccgactcgttcgccatgatccgcggcggccatatcgacctggcgatcctgggcggcatgga agtgtcgcagaacggcgacctggccaactggatgatcccgaagaagctgatcaagggcatgggcggcgccatggacctggtg catggcgcgaagaaggtcatcgtgatcatggaacactgcaacaagtacggcgagagcaaggtgaagaaggaatgctcgctgc cgctgaccggcaagggcgtcgtgcaccagctgatcaccgatctggccgtgttcgagttcagcaacaacgccatgaagctggtcg agctgcaggaaggcgtcagcctggaccaggtgcgcgaaaagaccgaggccgagttcgaggtgcatctgtga
adc	atgctgaaggacgaggtgatcaagcagatctcgaccccgctgacctcgccggcgttcccgcgcggcccgtacaagttccacaac cgcgagtacttcaacatcgtgtaccgcaccgacatggacgccctgcgcaaggtggtgccggaaccgctggaaatcgacgagcc gctggtgcgcttcgagatcatggccatgcacgacaccagcggcctgggctgctacaccgaaagcggccaggcgatcccggtgt cgttcaacggcgtgaagggcgactacctgcacatgatgtacctggacaacgaacccgcgatcgccgtgggccgcgaactgtcg gcctatccgaagaagctgggctacccgaagctgttcgtggactcggacaccctggtgggcaccctggactacggcaagctgcgc gtggccaccgccaccatgggctacaagcacaaggccctggacgccaacgaggccaaggaccagatctgccgcccgaactatat gctgaagatcatcccgaactacgacggctcgccgcgcatctgcgagctgatcaacgccaagatcaccgacgtgaccgtgcacga ggcctggacgggcccgacgcgcctgcagctgttcgatcatgccatggcgcccctgaacgacctgccggtgaaggaaatcgtgtc gtcgtcgcacatcctggccgacatcatcctgccgcgcgccgaagtgatctacgactatctgaagtga

Table S6. Flux Balance Analysis (FBA) systems biology prediction for autotrophic and heterotrophic synthesis of BDO using CO_2 & H_2 and guaiacol as sole energy and carbon sources respectively. The nominal experimental biomass growth rate of 0.0164 [h^{-1}] was use for both FBA simulations. Related to Figure 6 and Table 2.

Cell sources and sinks	Unit	Guaiacol as sole energy and carbon source	CO_2 and H_2 as sole energy and carbon source
Sources			
CO_2	[mmol/(gDCW·h)]		-3.0
H_2			-22.16
Guaiacol		-0.43	
O_2		-2.03	-7.2
P_i		-0.04	-0.04
SO_4^{2-}		-0.003	-0.003
NH_3		-0.17	-0.17
Sinks			
BDO[a]	[mmol/(gDCW·h)]	0.091	0.582
H_2O		0.95	18.94
CO_2		1.974	
Biomass	[h^{-1}]	0.0164	0.0164

[a]BDO is 2,3-butanediol.

Table S7. Summary of ASPEN HYSYS process simulations using a guaiacol feed basis of 1000 [kg/h] for the process flowsheets of Figure 9 and Figure 8, scaling the bioreactors for the guaiacol and CO_2 & H_2 fermentations using a design O_2 transfer rate of ~225 [mmol/(L·h)]. Related to Figures 8 and 9.

Sources and sinks	**Unit**	**Guaiacol as sole energy and carbon source**	**CO_2 and H_2 as sole energy and carbon source**
Guaiacol Feed Rate	[kg/h]	1000	1000
Gas Uptake Rates			
O_2	[mmol/(L·h)]	223	227
CO_2	[mmol/(L·h)]		82
H_2	[mmol/(L·h)]		669
Bioreactor Volume	[m^3]	200	100
2,3-butanediol Productivity			
Specific Productivity	[(kg BDO)/(m^3·h)]	0.79	1.48
Concentration [a]	[g/L]	30	30
Biomass			
Growth rate	[h^{-1}]	0.017	0.016
Dry Cell Weight	[g/L]	102	27
Operating costs			
Electricity demand	[kW]	2382	-566
Cooling water	[kW]	7702	-

[a] Controlled via microfiltration membrane.

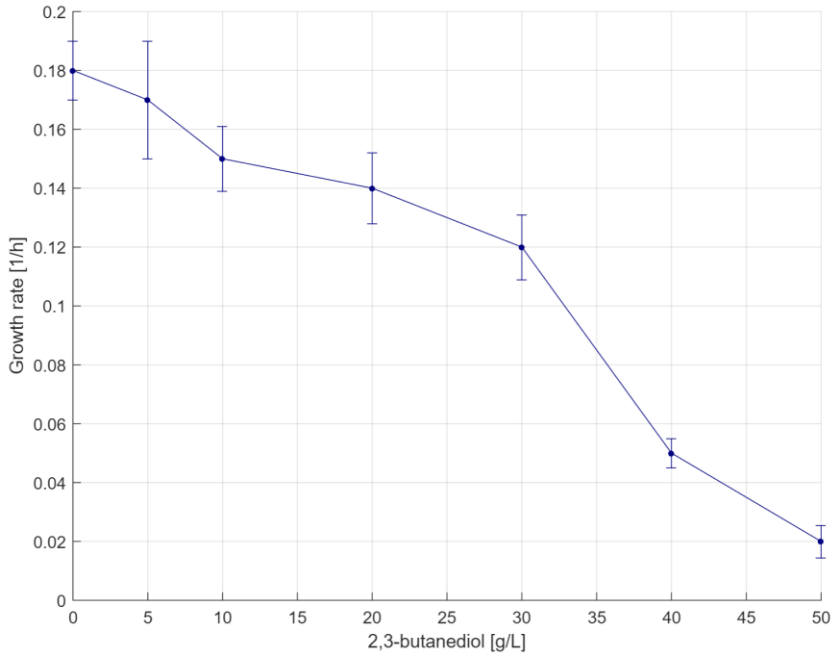

Figure S1. (A) BDO tolerance of *C. necator* H16 wild type, expressed as growth rate versus BDO concentration. Beyond a BDO concentration of 30 [g/L], the growth rate becomes significantly impaired. Related to Figure 1A.

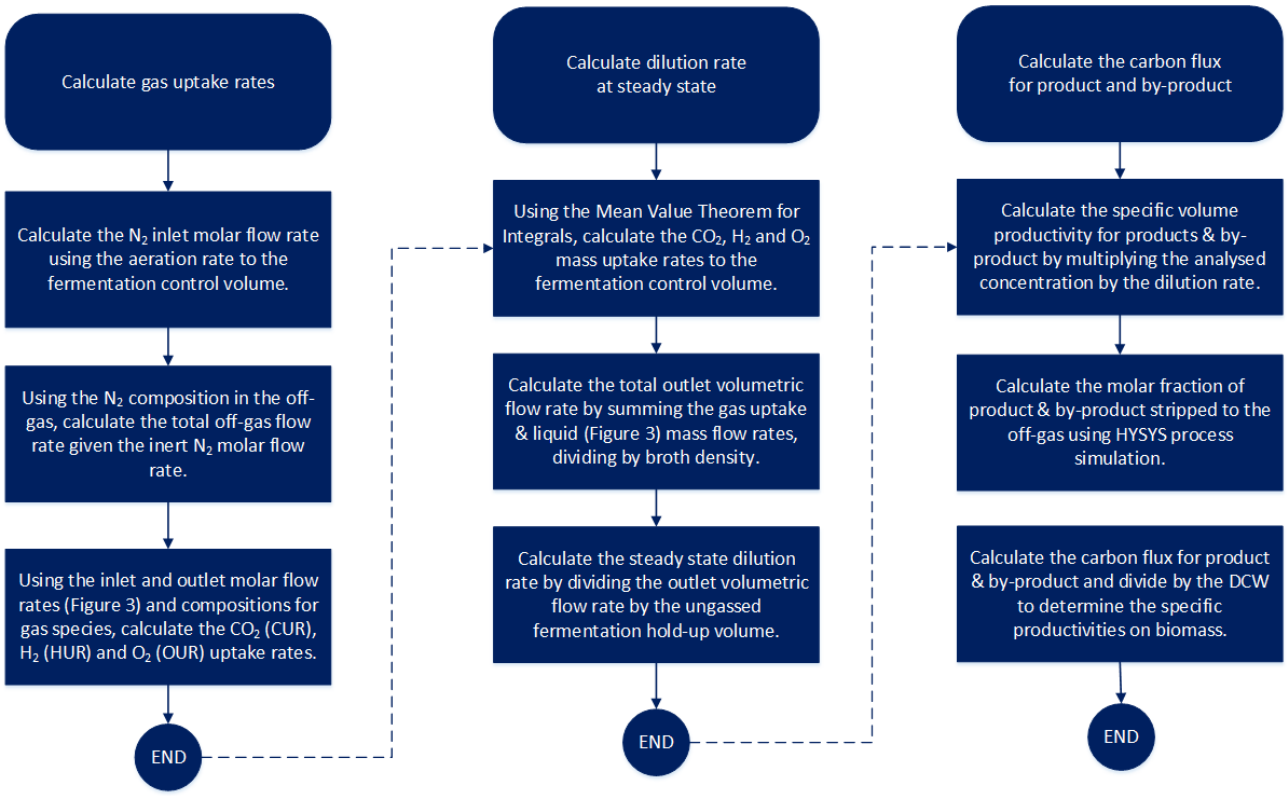

Figure S2. Methodology for calculating (1) gas uptake rates, (2) dilution rate at steady state and (3) product and by-product carbon flux for continuous, autotrophic fermentation. Related to Table 2 and Figures 4 and 5.

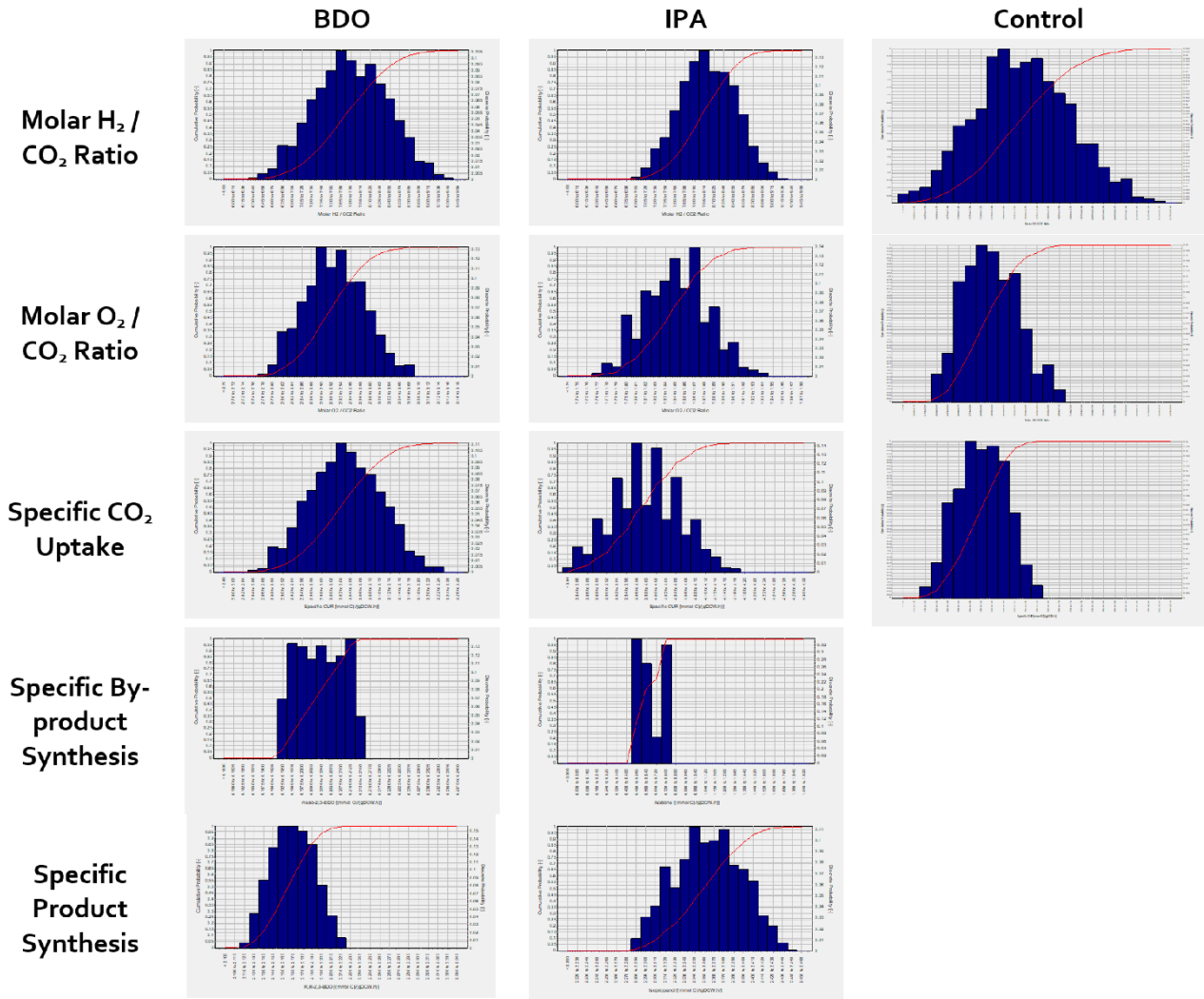

Figure S3. Monte Carlo simulations incorporating all sensor, analysis and calibration standard uncertainty into the respective calculated fermentation data. 90% confidence limits were determined from the cumulative probability curves. Related to Figure 4 and 5.

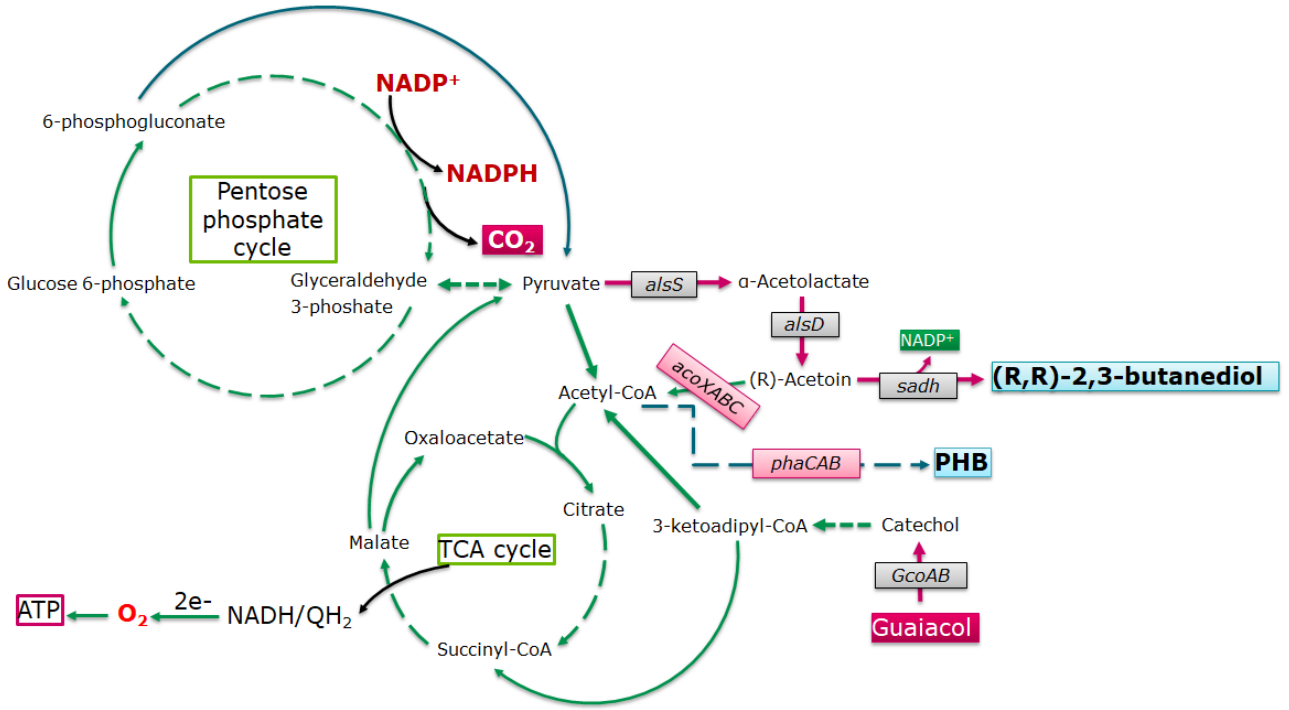

Figure S4. Biochemical network outlining the synthesis of (R,R)-2,3-butanediol from the lignin model compound, guaiacol, in the microbial cell factory, *C. necator* H16. Genes overexpressed to allow (R,R)-2,3-butanediol synthesis are contained in grey text boxes, whilst attenuated genes are contained in red text boxes. Guaiacol is demethylated to catechol and catabolised via the 3-oxoadipate pathway to succinyl-CoA and acetyl-CoA. Pyruvate is produced from malate via *malic enzyme* as the metabolite precursor to BDO synthesis. Related to Figures 8 and 9.